

Activation of osmo-sensitive LRRC8 anion channels in macrophages is important for micro-crystallin joint inflammation

Received: 4 November 2023

Accepted: 12 September 2024

Published online: 18 September 2024

Check for updates

Twinu Wilson Chirayath^{1,7}, Matthias Ollivier^{2,3,7}, Mete Kayatekin^{3,4,7}, Isabelle Rubera^{3,4}, Chinh Nghia Pham¹, Jonas Friard^{3,4}, Nathalie Linck^{2,3}, H elene Hirbec^{2,3}, Christ ele Combes⁵, Myl ene Zarka¹, Fr ed eric Liot e^{1,6}, Pascal Richette^{1,6}, Francois Rassendren^{2,3}, Vincent Compan^{2,3,8} , Christophe Duranton^{3,4,8} & Hang Korng Ea^{1,6,8}

Deposition of monosodium urate and calcium pyrophosphate (MSU and CPP) micro-crystals is responsible for painful and recurrent inflammation flares in gout and chondrocalcinosis. In these pathologies, the inflammatory reactions are due to the activation of macrophages responsible for releasing various cytokines including IL-1 . The maturation of IL-1  is mediated by the multi-protein NLRP3 inflammasome. Here, we find that activation of the NLRP3 inflammasome by crystals and concomitant production of IL-1  depend on cell volume regulation via activation of the osmo-sensitive LRRC8 anion channels. Both pharmacological inhibition and genetic silencing of LRRC8 abolish NLRP3 inflammasome activation by crystals *in vitro* and in mouse models of crystal-induced inflammation. Activation of LRRC8 upon MSU/ CPP crystal exposure induces ATP release, P2Y receptor activation and intracellular calcium increase necessary for NLRP3 inflammasome activation and IL-1  maturation. We identify a function of the LRRC8 osmo-sensitive anion channels with pathophysiological relevance in the context of joint crystal-induced inflammation.

Gout due to monosodium urate (MSU) crystal deposition, which occurs after chronic elevation of serum urate level, and calcium pyrophosphate (CPP) crystal deposition (also called chondrocalcinosis) are 2 major crystal-related diseases responsible for recurrent interleukin 1  (IL-1 )-orchestrated inflammation flares. Despite the availability of efficient urate-lowering drugs, gout remains active in more than 70% of patients, with continued gout flares^{1,2}. Moreover, current treatments of CPP disease are only symptomatic and not able to dissolve CPP crystals. IL-1  blockade is effective in reducing MSU and CPP

crystal-induced inflammation, but alternative therapies are still needed because prolonged IL-1  blockade is associated with severe side effects such as infections and MSU and CPP crystal-induced inflammation can be resistant to IL-1  blockade³.

MSU and CPP crystals induce the release of IL-1  by resident macrophages⁴. Production of active IL-1  occurs via the activation of the multiprotein complex nucleotide-binding domain and leucine-rich repeat pyrin 3 domain (NLRP3) inflammasome. NLRP3 oligomerizes and assembles with Apoptosis-associated Speck-like protein

¹Universit e Paris Cit e, INSERM UMR-1132, Bioscar, H opital Lariboisi ere, AP-HP, Paris, France. ²Institut de G enomique Fonctionnelle, Universit e de Montpellier, CNRS, INSERM, 34094 Montpellier, France. ³Laboratory of Excellence Ion Channels, Science & Therapeutics, F-06560 Valbonne, France. ⁴Universit e C ote d'Azur, CNRS, LP2M, Nice, France. ⁵Universit e Toulouse, ENSACIET, INPT-CNRS, F-31000 Toulouse, France. ⁶H opital Lariboisi ere, AP-HP, Rheumatology department, Centre Viggo Petersen, DMU Locomoteur, Paris, France. ⁷These authors contributed equally: Twinu Wilson Chirayath, Matthias Ollivier, Mete Kayatekin. ⁸These authors jointly supervised this work: Vincent Compan, Christophe Duranton, Hang Korng Ea. e-mail: vincent.compan@igf.cnrs.fr; christophe.duranton@univ-cotedazur.fr; hang-korng.ea@aphp.fr

containing a caspase activation and recruitment domain (CARD) (ASC) to form an active inflammasome leading to caspase-1 activation, which in turn cleaves pro-IL-1 β into mature IL-1 β that is released from the cell⁵. NLRP3 inflammasome can be activated by different stimuli including sterile molecules such as extracellular adenosine triphosphate (ATP) or nanoparticles (for review see ref. 6). In macrophages, a decrease in extracellular osmolarity (hypotonic challenge) and the subsequent regulatory volume decrease (RVD) phenomenon also leads to NLRP3 inflammasome activation^{7,8}. In mammalian cells, the RVD mechanism counteracts the decrease in extracellular osmolarity by a compensatory mechanism leading to the loss of K⁺/Cl⁻ ions and osmotically obliged water. This massive loss of osmolytes results from the simultaneous activation of potassium channels and volume-regulated anion channels (VRACs). The ubiquitously expressed leucine-rich repeat-containing 8 (LRRC8) anion channel family has been identified as the main molecular component of the VRAC^{9,10}. These channels are activated during low osmolarity exposure and trigger the RVD process by extruding Cl⁻ and osmolytes¹¹, thus allowing for recovery of normal cell volume. The LRRC8 family contains 5 subunits, LRRC8A to E, which form heteromeric channels¹²⁻¹⁴. The LRRC8A subunit is the mandatory subunit to form functional channels¹⁰. Recently, in macrophages, LRRC8 channels were demonstrated to be essential for hypotonic-induced NLRP3 activation and IL-1 β secretion¹⁵.

In macrophages, MSU and CPP crystals induce NLRP3 activation via several cellular disturbances including reactive oxygen species production, autophagy alterations and metabolism modifications¹⁶. Previous works suggested that phagocytosed MSU crystals can be dissolved in phagolysosomes, thereby leading to an intracellular increase in osmolarity and subsequent osmolarity-driven water influx responsible for the decrease in intracellular potassium concentration.

Despite these data, the role of LRRC8A in MSU crystal-induced IL-1 β production is unknown. Here we show in humans and in mouse models that cell volume changes play a central role in inflammasome activation upon macrophage exposure to MSU/ CPP crystals. Crystal exposure triggers LRRC8 activation and subsequent ATP efflux, both necessary for NLRP3 inflammasome activation via P2Y purinergic receptor and intracellular calcium signalling.

Results

In humans, high IL-1 β concentration is associated with decreased synovial fluid (SF) osmolarity during gout and CPP flares

The identification of MSU and CPP crystals on compensated polarized light microscopy of human SF with high cell concentration (>2000/mm³) established the diagnosis of gout and CPP flares, respectively. The diagnosis of osteoarthritis (OA) was based on clinical, SF with low cell concentration (<1000/mm³) and radiography patterns (Supp. Fig. 1a). We excluded OA associated with CPP crystals identified in SF. The osmolarity of SFs was lower during gout (MSU) and chondrocalcinosis (CPP) flares than that for OA (Fig. 1a). Crystal (Cryst.) refers to all values for patients with gout- and CPP-mediated diseases. Levels of IL-1 β (Fig. 1b) and IL-8 (Fig. 1c) were higher in MSU and CPP than OA SFs. We found a negative correlation between the osmolarity of SF and concentration of IL-1 β and IL-8 (Fig. 1d, e), with IL-1 β and IL-8 level increased with decreasing osmolarity. There was also a mild negative correlation between SF osmolarity and SF cell concentration (Supp. Fig. 1b). All these results suggest that SF osmolarity modulates MSU and CPP crystal-induced IL-1 β /IL-8 production.

Microcrystal-induced inflammation depends on osmolarity and cell water flux in mouse model

To explore the putative contribution of osmolarity changes in the modulation of the microcrystal-induced inflammation, we used the *in vivo* mouse air pouch model (Fig. 2a). The air pouch cavity mimics a

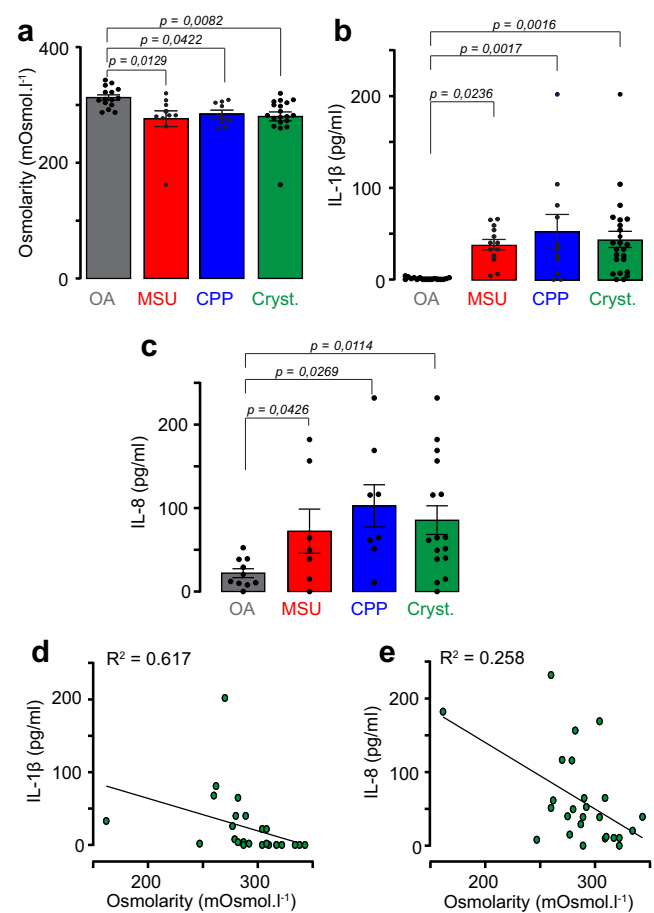


Fig. 1 | Presence of MSU or CPP crystals in human synovial fluids is associated with low osmolarity and IL-1 β release. a–c osmolarity (a, $n = 15$ OA, 10 MSU, 9 CPP) IL-1 β level (b, $n = 17$ OA, 13 MSU, 11 CPP) and IL-8 (c, $n = 10$ OA, 6 MSU, 8 CPP) level measured in the SF of osteoarthritis (OA), MSU and CPP disease. d, e Correlation between IL-1 β (d), IL-8 (e) level and SF osmolarity ($n = 25$ paired samples). Crystal (Cryst.) refers to all values obtained for gout and CPP diseases. Values are mean \pm SEM. Multiple comparisons by one-way ANOVA (a–c). R² coefficients were calculated with the Spearman test (d, e).

joint cavity with a lining structure resembling the synovial membrane, formed as early as 6 days after air pouch creation¹⁷. Crystal-induced inflammation in this model reproduces the different phases of MSU and CPP flares observed in patients with a self-limited reaction¹⁸. Using this model, we artificially increased mouse plasma osmolarity by intraperitoneal injection of mannitol 20% (-1 ml, Pos -1050 mOsm.l⁻¹), a non-charged osmolyte. After 3 consecutive days of mannitol injection, plasma osmolarity increased to 321 mOsm.l⁻¹. Mice receiving phosphate buffered saline (PBS) showed normal plasma osmolarity, 298 mOsm.l⁻¹ (Fig. 2b). Mannitol treatment strongly reduced microcrystal-induced inflammation (with both MSU and CPP crystals), as evidenced by the decrease in air pouch membrane inflammation score, number of cells collected and IL-1 β level measured in air pouch lavage (Fig. 2c–f).

To balance osmolarity challenge and cellular swelling, cells facilitate water exchange through aquaporin channels. Therefore, we used mercury chloride (IP injection, HgCl₂, 10 μ g/g) to block aquaporin channels¹⁹. Aquaporin inhibition completely abolished inflammation induced by MSU and CPP crystals by reducing the inflammation score, number of cells and level of IL-1 β collected in lavage (Fig. 2g–j). Aquaporin blockade also reversed the ratio of macrophages to neutrophils to the same proportion as observed in PBS-treated mice (supp. Fig. 2a, b, supp Fig. 7a, b).

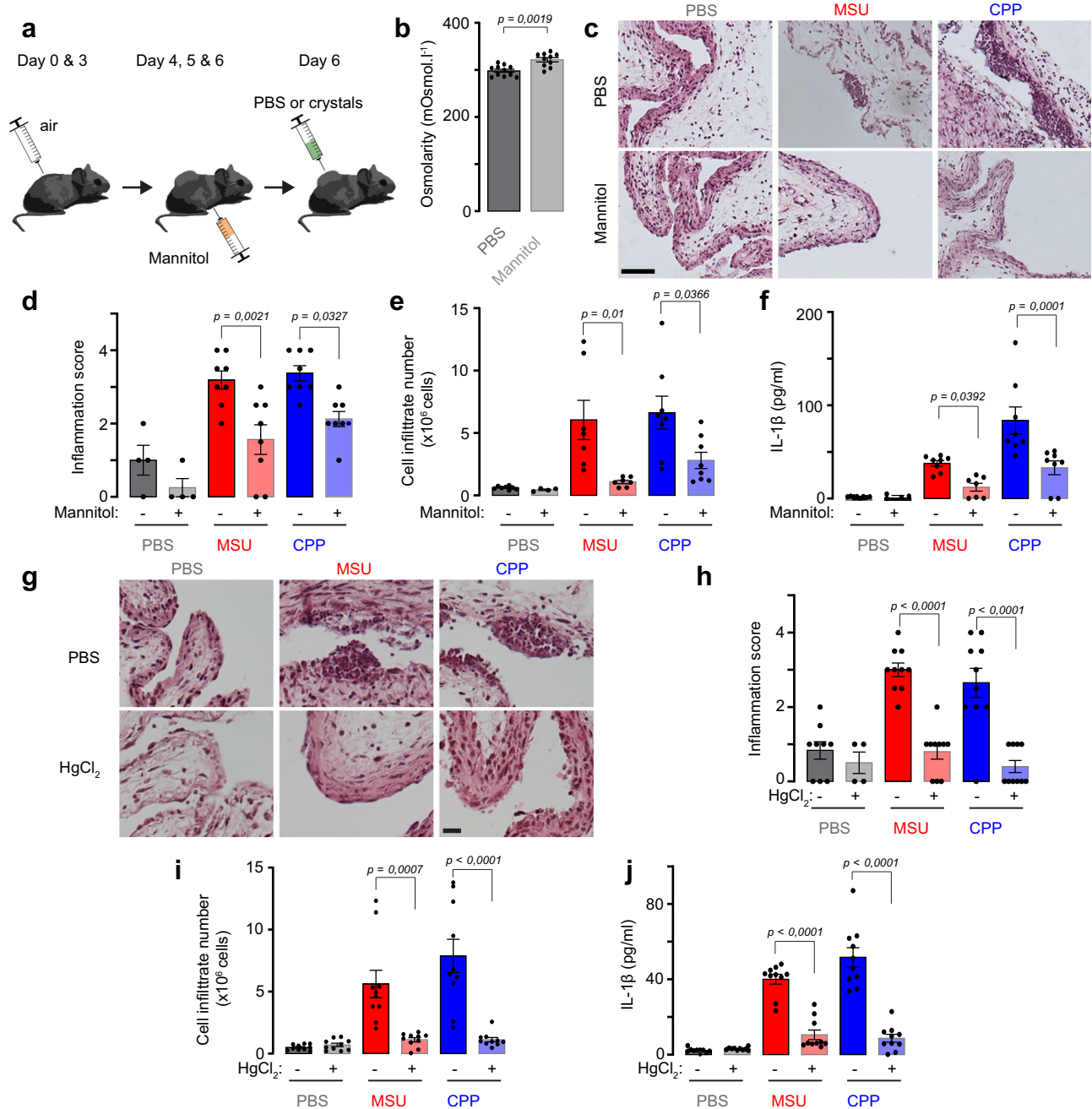


Fig. 2 | Level of inflammation in in vivo microcrystal-induced mouse air pouch model depends on osmolarity and cell water flux. **a** Air pouch was created by injection of 3 ml sterile air in subcutaneous dorsal area on days 0 and 3. On day 6, sterile MSU or CPP crystals (1 mg in 1 ml PBS) or PBS were injected into the air pouch and inflammation was assessed 6 h later by quantifying cytokine levels and cell infiltration in the lavage solution. **b** Plasma osmolarity (in mOsm.l^{-1}) measured in mice receiving intraperitoneal injection of PBS (isotonic, 300 mOsm.l^{-1} , $n = 11$ mice) or 1 ml mannitol 20% (hypertonic 1050 mOsm.l^{-1} , $n = 10$ mice) every day from day 4 to 6. **c, d** Representative micrographs (**c**, HE staining) and semi-quantitative inflammation score (**d**) of air pouch membranes obtained from control ($n = 4$) and mannitol-treated mice receiving PBS, or MSU or CPP crystal injection ($n = 8$ mice/group). Scale bar, $40 \mu\text{m}$. **e, f** cell infiltration numbers (**e**) ($n = 8$ mice PBS, 6

mannitol, 7 MSU and MSU+mannitol, 8 CPP and CPP+mannitol) and IL-1 β concentrations (**f**, ELISA quantification) ($n = 8$ mice in PBS, MSU, CPP and CPP+mannitol, 6 in mannitol, 7 MSU+mannitol) measured in the air pouch lavage. **g, h** Representative micrographs (**g**) and semi-quantitative inflammation score (**h**) of the air pouch membranes obtained from control and intraperitoneal mercury (HgCl_2)-treated mice receiving PBS, or MSU or CPP crystal injection ($n = 4$ mice in HgCl_2 , 9 PBS, 10 in MSU and CPP crystal groups). Scale bar, $20 \mu\text{m}$. **i, j** Cell infiltration numbers (**i**) and IL-1 β level (**j**) measured in air-pouch lavage collected from the mouse groups treated or not with mercury ($n = 10$ mice/per group). Values are mean \pm SEM. Two-tailed unpaired t-test (**b**), two-way ANOVA with Sidak's multiple comparisons test (**c–j**).

Next, we confirmed in vitro that aquaporin inhibition (HgCl_2) reduced microcrystal-induced IL-1 β production in both the monocytic primed THP-1 cell line and primed bone marrow-derived macrophages (BMDMs) (supp. Fig. 2c, d). In THP-1 cells, HgCl_2 treatment also prevented microcrystal-induced speck formation by ASC (supp. Fig. 2e)

and NF- κB activation (supp. Fig. 2f). We also found reduced release of 2 cytokines independent of NLRP3 activation, IL-8 and tumor necrosis factor α (TNF) (supp. Fig. 2g, h). These results support that the anti-inflammatory effects of HgCl_2 were both inflammasome-dependent and -independent. To determine whether crystal-induced NF- κB

activation is independent of NLRP3, we treated THP-1 cells with the NLRP3 inflammasome inhibitor MCC950 and assessed NF- κ B activity and IL-1 β production under crystal stimulation. MCC950 did not affect NF- κ B activation while effectively inhibited IL-1 β production (supp. Fig. 2i, j). These findings suggest that NF- κ B activation is independent of NLRP3 inflammasome activation and that NF- κ B activation by crystals is not a paracrine effect of IL-1 β secretion induced by crystals.

Cell volume changes and LRRC8 channels mediate NLRP3 inflammasome activation and IL-1 β secretion during crystal exposure

We next deciphered the mechanisms underlying the effect of osmolarity on crystal-induced IL-1 β inflammation in monocytic THP-1 cells and the contribution of the osmo-sensitive LRRC8 channels in this process. LRRC8 are activated by a decrease in extracellular osmolarity (hypotonicity, <300 mOsm.l⁻¹) and conversely inhibited by an increase in extracellular osmolarity (hypertonicity; >300 mOsm.l⁻¹). As a result, a hypertonic solution obtained by adding 100 mOsm.l⁻¹ of mannitol to isotonic PBS medium (Mannitol, osmolarity increased to ~400 mOsm.l⁻¹ without modification of ion concentrations) greatly decreased MSU and CPP crystal-induced IL-1 β production (200 μ g/ml, 3 h, Fig. 3a). Similarly, the addition of DCPIB (20 μ M) to isotonic PBS medium, a known and specific inhibitor of LRRC8 channels^{20,21}, inhibited the production of IL-1 β induced by both MSU and CPP crystals (Fig. 3b), which suggests that crystal exposure activated LRRC8 channels. To ensure that adding crystals (MSU or CPP) did not alter the osmotic pressures of the bath solutions, we measured the osmolarity after a 6-hours incubation with or without THP-1 cells. The results showed no change in osmolarity across hypotonic, isotonic, or hypertonic solutions, regardless of crystal addition or cell presence (supp. Fig. 3a).

Measurement of cell volume changes (using calcein self-quenching fluorescence method²⁰) showed that the addition of MSU or CPP crystals induced rapid cell swelling followed by decreased cell volume that was faster with CPP than MSU crystals (Fig. 3c, d), whereas under iso-osmotic conditions and in the absence of crystals, the cell size remained constant and stable for 120 min (Fig. 3c). As expected, DCPIB (20 μ M) treatment did not prevent the cell swelling but significantly reduced the cell shrinkage (Fig. 3c, d and supp. Fig. 3b, c). DCPIB also greatly decreased MSU and CPP crystal-induced NF- κ B activation as well as TNF production and ASC speck formation (supp. Fig. 3d–f).

All these results support a contribution of LRRC8 in microcrystal-induced inflammation. To test this hypothesis, we stably knocked down the expression of LRRC8A, the mandatory subunit of VRAC channels¹⁰, in THP-1 cells by using a lentiviral-based shRNA strategy, silencing LRRC8A expression by more than 80% as compared with parental control cells (Fig. 3e, f). Patch-clamp whole-cell recordings performed using NMDGCl pipette and bath solutions (Fig. 3g) revealed that in LRRC8A-KD cells, the volume-activated chloride currents evoked by hypotonic conditions (220 mOsm.l⁻¹) were decreased by 85% as compared with control cells (current densities measured at -100 mV were -64 ± 13 pA/pF and -9.7 ± 1 pA/pF, for control and LRRC8A-KD, respectively). DCPIB (20 μ M) treatment completely abolished the hypotonic-activated chloride currents in both control and LRRC8A-KD cells. Cell volume measurement confirmed that RVD evoked by hypotonic challenge was impaired in LRRC8A-KD cells (supp. Fig. 3g). Hypotonicity-induced ASC speck formation (Fig. 3h, i, 100 mOsm.l⁻¹, 1 h), as well as hypotonic-mediated IL-1 β processing and release (Fig. 3j, k, 100 mOsm.l⁻¹, 1 h), were also decreased in LRRC8A-KD cells. Importantly, LRRC8A silencing did not affect the cellular expression of ASC, NLRP3 and pro-IL-1 β proteins (Fig. 3j) nor the activation of AIM2 inflammasome induced by Poly(dA:dT). Similarly, in BMDMs, pharmacological inhibition of LRRC8 (with DCPIB) impaired volume-activated chloride currents, cell volume change and IL-1 β release

after hypotonic challenge (supp. Fig. 4a–c). Expressions of *Lrrc8* and *Tmem16* subunits were not modified by LPS treatment of BMDMs (supp. Fig. 4a–d), while knockdown of *Lrrc8A* significantly decreased IL-1 β release after hypotonic challenge without affecting the expression of the other *Lrrc8* and *Tmem16f* subunits (supp. Fig. 4d–f).

Finally, in THP-1 cells, we explored the contribution of the LRRC8 channels in crystal-induced NLRP3 inflammasome activation. After MSU or CPP crystal exposure, both IL-1 β release (Fig. 3l), number of ASC speck-positive cells (Fig. 3m) and RVD (Fig. 3n and supp. Fig. 5a–c) were strongly impaired in LRRC8A-KD cells. These data support that NLRP3 inflammasome activation and IL-1 β secretion during crystal exposure require LRRC8 anion channels.

Lrrc8A ablation in monocyte/macrophage lineage prevents microcrystal-induced inflammation in vivo and in vitro

To further investigate the implication of LRRC8 channels in microcrystal-induced inflammation, *Lrrc8A* was specifically invalidated in the monocyte/macrophage lineage in *Cx3Cr1^{CreERT2}/Lrrc8A^{fl/fl}* mice^{22,23}. This conditional model contains a Cre recombinase fused to a mutant estrogen ligand binding domain (CreERT2) that is activated by the estrogen antagonist tamoxifen. Upon tamoxifen injection, *Cx3Cr1*-expressing cells (i.e., the monocyte/macrophage lineage) invalidate *Lrrc8A* expression. In this model microcrystal-evoked inflammation was induced in the air pouch model after tamoxifen treatment. FACs analysis of air pouch lavage showed that LRRC8A expression was lower in macrophages from tamoxifen-treated *Cx3Cr1^{CreERT2}/Lrrc8A^{fl/fl}* mice (hereafter *Lrrc8A^{ΔMo}* mice) than tamoxifen-treated *Cx3Cr1^{CreERT2}* mice (hereafter *Lrrc8A^{cont}* mice) (Fig. 4a). Inflammation induced by MSU and CPP microcrystals in the air pouch was greatly inhibited in *Lrrc8A^{ΔMo}* mice as compared with *Lrrc8A^{cont}* mice as demonstrated by reduced IL-1 β level, cell infiltration and inflammation score (Fig. 4b–g). Finally, in BMDMs isolated from *Cx3Cr1^{CreERT2}/Lrrc8A^{fl/fl}* mice, tamoxifen treatment decreased LRRC8A expression (Fig. 4h) and IL-1 β production induced by MSU and CPP crystal exposure (Fig. 4i). These results identified the LRRC8A subunit as a major actor in MSU and CPP crystal-induced inflammation.

Hypotonic and crystal activation of LRRC8 mediates ATP release by macrophages

We next investigated the mechanisms by which LRRC8 can regulate NLRP3 inflammasome activation. We focused on ATP signaling because purinergic receptors have been found involved in crystal-evoked inflammation²⁴. Control THP-1 cells exposed to a hypotonic challenge (100 mOsm.l⁻¹) showed a significant release of ATP in the supernatant (15 min, Fig. 5a) as compared to isotonic condition (300 mOsm.l⁻¹). This ATP release was strongly inhibited by DCPIB (20 μ M) or in LRRC8A-KD THP-1 cells, which suggests a major role of LRRC8 in hypotonic-mediated ATP release (Fig. 5a). To temporally characterize this ATP release in the THP-1 cell population, we used a recently developed ATP fluorescent biosensor called PNG6²⁵ (Fig. 5b). We first confirmed that this biosensor was functional. THP-1 cells expressing PNG6-P2A-Scarlet sensed extracellular ATP dose-dependently, whereas those expressing PKG6, a dead mutant of the sensor, did not show any fluorescence upon ATP stimulation (supp. Fig. 5d, e). In THP-1 cells expressing PNG6-P2A-Scarlet hypotonic challenge (160 mOsm.l⁻¹) induced a transient and massive release of ATP that peaked at -10 min and decreased to the basal level within 20 min (Fig. 5c). DCPIB (20 μ M) or LRRC8A-KD abolished ATP-evoked fluorescence without affecting biosensor activation, as assessed by a final stimulation with 10 μ M ATP (Fig. 5c, supp. Fig. 5f). Because LRRC8 channels are permeant to small anionic molecules, we evaluated whether they might be permeable to ATP. To that aim, we used patch-clamp whole-cell recording in THP-1 cells with Na₂ATP in both bath and pipette solutions. In these conditions, exposure to hypotonic solution rapidly (<5 min; 260 mOsm.l⁻¹) induced ATP-driven currents at

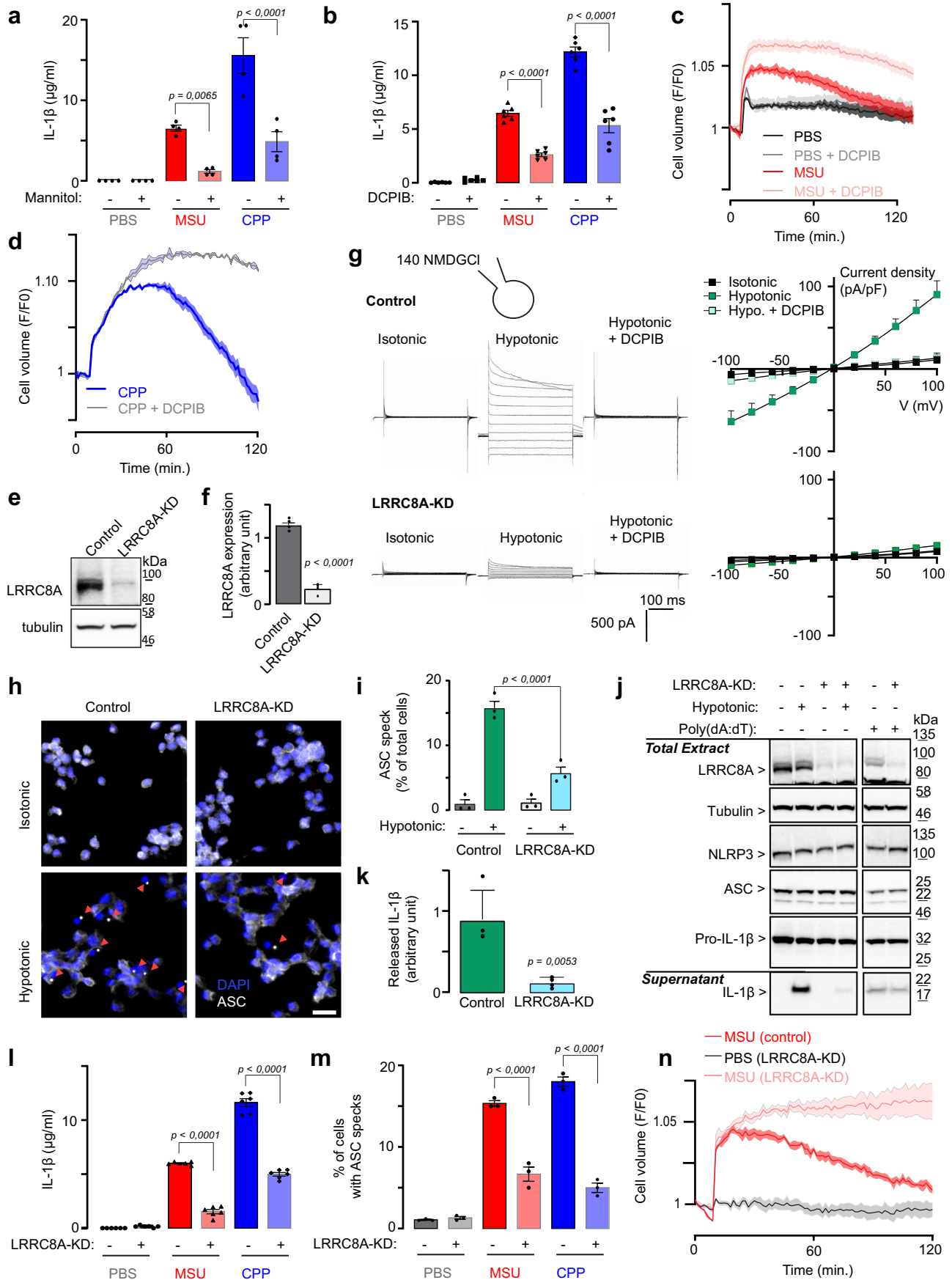


Fig. 3 | LRRCS channels mediate NLRP3 inflammasome activation and IL-1 β secretion during crystal exposure in THP-1 macrophages. **a, b** IL-1 β release in supernatants of primed THP-1 cells stimulated with crystals in isotonic (PBS) or hypertonic solutions (mannitol) (**a**, $n = 4$ independent experiments) and in isotonic with/without DCPIB (**b**, $n = 6$ independent experiments). **c, d** Cellular volume change measured in THP-1 cells induced by PBS alone or PBS containing MSU (**c**) or CPP (**d**) with/without DCPIB, $n = 4$ independent experiments. **e, f** LRRCSA protein expression level in control and LRRCSA-KD THP-1 cells ($n = 5$ independent preparations). **g** Chloride whole-cell currents in control (upper panel) and LRRCSA-KD (lower panel) THP-1 cells recorded successively with isotonic and hypotonic solution (5 min) and in the presence of DCPIB. Pipette and bath solutions contained NMDG-Cl. The corresponding I/V curves calculated with isotonic solution (black), hypotonic solution (green) and with DCPIB (light green) are depicted on the right. ($n = 22$ and 9 independent recordings for control and LRRCSA-KD THP-1 cells,

respectively). **h, i** Micrographs illustrating the ASC speck formation (**h**) and percentage of cells containing ASC speck (**i**, $n = 4$ independent experiments) detected in control and LRRCSA-KD cells maintained in isotonic or hypotonic solutions. Red arrows indicate the ASC specks. Scale bar 30 μm . **j** Western blot analysis of NLRP3 inflammasome components and supernatant IL-1 β release in control and LRRCSA-KD THP-1 cells after exposure to a hypotonic solution or a Poly(dA:dT) stimulation. **k** Quantification of IL-1 β release in supernatant of control and LRRCSA-KD cells after hypotonic exposure ($n = 3$ independent experiments). **l, m** IL-1 β release (**l**) and percentage of cells containing ASC speck (**m**) measured in control and LRRCSA-KD cells after MSU and CPP exposure ($n = 6$ and 3 independent experiments). **n** Cellular volume change measured in control and LRRCSA-KD cells after MSU crystal exposure. ($n = 9$ independent experiments). All values are mean \pm SEM. Two-tailed unpaired t-test (**e, f, k**), two-way ANOVA, Sidak's multiple comparisons test (**a, b, i, l, m**).

negative and positive holding potentials, corresponding to an efflux and influx of negative charges, respectively (Fig. 5d, e). The mean ATP current densities evoked by the hypotonic condition were -20.0 ± 2.0 pA/pF ($n = 6$) and -8.1 ± 2.1 pA/pF (measured at -100 mV, Fig. 5f) in the absence or presence of DCPIB (20 μM), respectively, supporting the idea that LRRCS channels exhibit ATP conductance.

We next investigated at the single cell level a possible relation between hypotonic-evoked ATP release and RVD. Using time-lapse microscopy on THP-1 cells stably expressing PNG6-P2A-Scarlet, we simultaneously recorded ATP release and cell surface changes during hypotonic challenge (100 mOsm.l $^{-1}$) by measuring the Scarlet signal as a readout of cellular volume (Fig. 5g). Most of the cells initiated their RVD phase and released ATP during the first 10 min after the hypotonic challenge (Fig. 5h). Importantly, we observed only one event of ATP release per cell during the recording period. Genetic silencing of LRRCSA (LRRCSA-KD) completely prevented ATP release as well as RVD at the single cell level (Fig. 5h). We next analyzed the occurrence of the ATP release event and the initiation of RVD. The ATP release event occurred only during the swelling phase and concomitantly with the initiation of the RVD phase (Fig. 5i). We found a high correlation between the 2 events, with a correlation coefficient > 0.97 (Fig. 5j). These results suggest that ATP release via LRRCS is the triggering event leading to RVD.

Finally, we tested the putative contribution of LRRCS in ATP release on crystal exposure in THP-1 cells. ATP release in the supernatants was significantly increased after MSU or CPP crystals exposure (200 $\mu\text{g/ml}$, 3 h) and was blunted by DCPIB or in LRRCSA-KD THP-1 cells (Fig. 5k). These results support that MSU and CPP crystals trigger LRRCS-dependent extracellular ATP release.

LRRCS-evoked ATP release governs the RVD and NLRP3 inflammasome activation via P2YR signaling

We next analyzed the contribution of purinergic receptor signaling to RVD and inflammasome activation in THP-1 cells. Incubation with 20 units/mL apyrase, an extracellular ATP/ADP-hydrolyzing enzyme, prevented hypotonicity-induced RVD (Fig. 6a) and IL-1 β production (Fig. 6b). This effect was dose-dependent and observed with different grades of apyrase (Fig. 6b, c). Using BMDM from P2X7 $^{-/-}$ mice we showed that MSU and CPP crystal-evoked IL-1 β production was not impaired, ruling out the contribution of P2X7 receptors (supp. Fig. 6). Because P2X receptors are not involved in hypotonicity-evoked inflammasome activation⁷, we tested a potential contribution of different P2Y receptors to RVD and IL-1 β release. The P2Y2 receptor antagonist ARC118925 inhibited RVD to almost the same extent as LRRCSA-KD, whereas antagonists of P2Y1, P2Y6, and P2Y11 had no effect (Fig. 6d). Both P2Y2 and P2Y6 antagonists inhibited hypotonicity-induced IL-1 β release (Fig. 6e, f), yet without affecting hypotonicity-evoked ATP release (supp. Fig. 5g). P2Y1 and P2Y11 antagonists had no effect (Fig. 6f). Accordingly, in THP-1 cells, MSU and CPP crystal-induced IL-1 β release was strongly reduced with P2Y2 and P2Y6

antagonist application (Fig. 6g). Finally, using the air pouch model, in vivo inhibition of P2Y6 greatly decreased the MSU and CPP crystal-induced inflammation score, immune cell infiltration and IL-1 β release (Fig. 6h–k).

P2YR signaling evokes intracellular calcium increase and IL-1 β release

We next investigated the intracellular signaling pathways downstream of P2Y receptor activation, focusing on intracellular calcium, which is involved in NLRP3 inflammasome activation²⁶. To address this, we used single cell time-lapse microscopy on human THP-1 cells stably expressing the cytoplasmic calcium indicator GCaMP6s and the fluorescent reporter mScarlet (Fig. 7a). Our recordings of hypotonicity-evoked intracellular calcium variations revealed that hypotonicity induced a significant burst in intracellular calcium levels, peaking approximately 10 minutes after the reduction of extracellular osmolarity (Fig. 7a). This major calcium increase was abolished by silencing LRRCSA or inhibiting the P2Y2 receptor with 10 μM ARC118925 (Fig. 7a, b). Though, inhibition of P2Y2 by ARC118925, P2Y6 by MRS2578 or NLRP3 by MCC950, did not significantly affect the hypotonic-induced VRAC conductance in control THP-1 cells (Fig. 7c). Together these data support that intracellular calcium signaling evoked by hypotonicity results from VRAC activation and subsequent ATP release and P2YR activation. Single-cell analysis of both intracellular calcium signals and cell surface dynamics indicated that most cells exhibited at least one burst of intracellular calcium concomitant with the initiation of the RVD phase following hypotonicity challenge (Fig. 7d, e), in accordance with ATP release events shown in Fig. 5i. A significant correlation was observed between the time to RVD and the time to maximal calcium peak ($R^2 > 0.5$, $p < 0.001$, $n = 70$ paired, Fig. 7f) suggesting a role of intracellular calcium signaling in RVD initiation.

P2Y2 and P2Y6 are Gq-coupled GPCRs that both activate the phospholipase C (PLC) pathway, resulting in Ca $^{2+}$ release from intracellular stores (Fig. 7g). We found that, in THP-1 cells, U73122, a PLC inhibitor, suppressed MSU and CPP crystal-induced IL-1 β release (Fig. 7g), whereas U73343, an inactive analog of U73122, did not. Altogether, these data support that LRRCSA-evoked ATP release promotes autocrine and/or paracrine activation of P2Y2 and P2Y6 receptors, leading to subsequent intracellular calcium signaling and inflammasome activation.

Discussion

In this study, we identified LRRCS channels and cell volume regulation as central orchestrators of MSU and CPP crystal-induced inflammation in both human and mouse macrophages (Fig. 8). MSU and CPP crystals induce cell swelling followed by a LRRCSA-dependent RVD response, a cellular phenomenon mimicking hypotonic challenge. Crystal-mediated LRRCS activation leads to ATP release which in turn activates P2Y2 and P2Y6 purinergic receptors and the subsequent

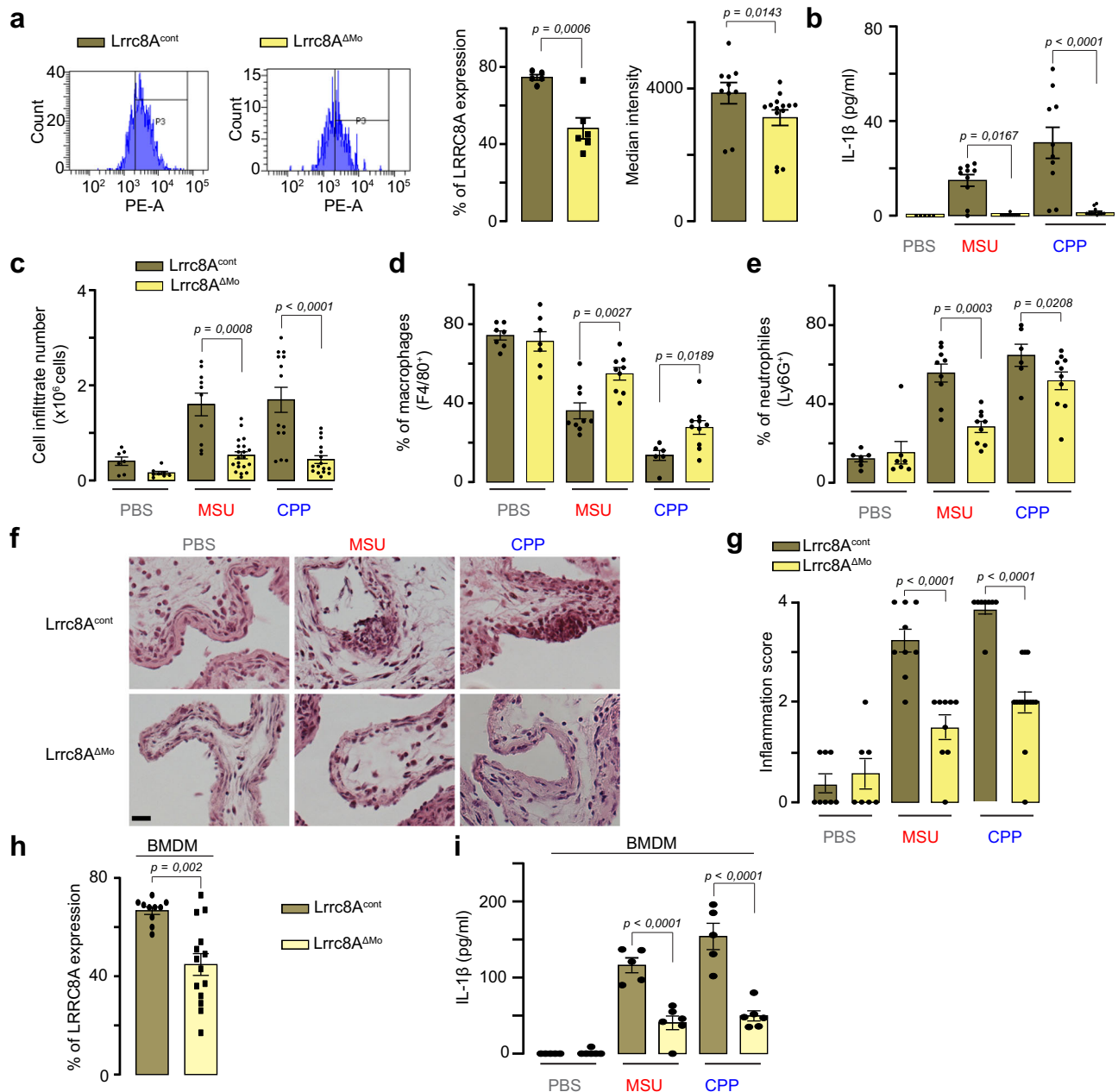


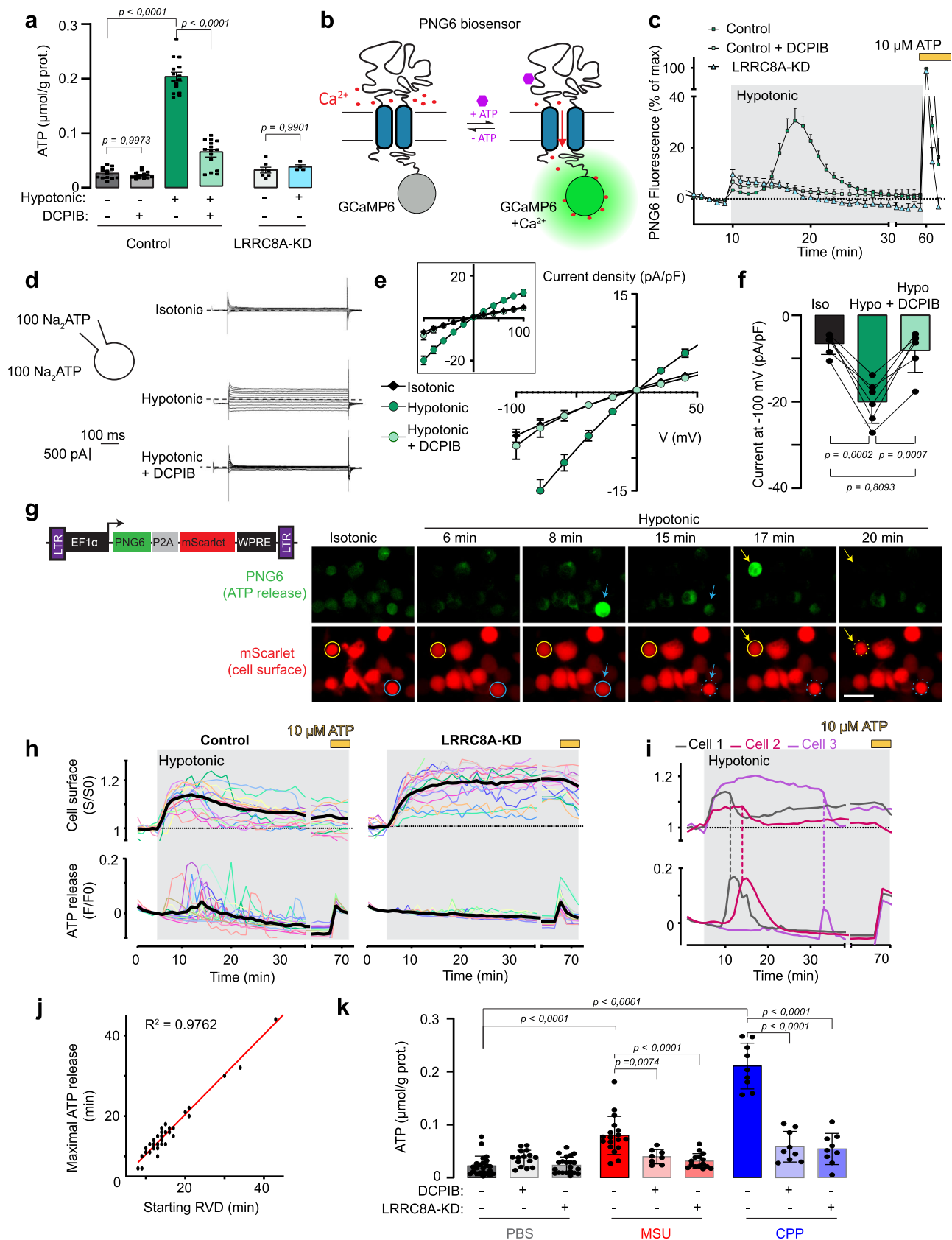
Fig. 4 | Deletion of *Lrrc8A* in monocyte/macrophage lineage abolishes microcrystal-induced inflammation in in vivo experiments. **a** Percentage of macrophages expressing LRRc8A assessed by FACS (left, representative expression of each group; middle and right, mean \pm SEM). Cells collected from air pouch lavage from *Lrrc8^{cont}* and *Lrrc8^{ΔMo}* mice were stained with antibody against F4/80 and LRRc8A ($n = 10$ *Lrrc8^{cont}*, and $n = 14$ *Lrrc8^{ΔMo}* mice). **b–e** *Lrrc8A* deletion in macrophage lineage reduced inflammation in air pouch model: IL-1 β level quantified by ELISA (**b**, $n = 7/9/10$ WT mice PBS/MSU/CPP, $8/10/11$ *Lrrc8^{ΔMo}* PBS/MSU/CPP); cell infiltration number (**c**, $n = 7/10/14$ WT mice PBS/MSU/CPP, $8/20/16$ *Lrrc8^{ΔMo}* PBS/MSU/CPP); percentage of macrophages (**d**) and neutrophils (**e**) assessed by FACS

measured in air pouch lavage ($n = 7/9/6$ WT mice PBS/MSU/CPP, $7/9/9$ *Lrrc8^{ΔMo}* PBS/MSU/CPP). **f** Representative air pouch membrane histology after HE staining and **(g)** air pouch membrane semi-quantitative inflammation score ($n = 8/9/8$ WT mice PBS/MSU/CPP, $7/9/14$ *Lrrc8^{ΔMo}* PBS/MSU/CPP). Scale bar, 20 μ m. **h**, *Lrrc8A* deletion in BMDMs reduced LRRc8A expression (**h**) and IL-1 β production (**i**), quantified by FACS and ELISA, respectively, in supernatant of BMDM isolated from *Cx3Cr1^{CreERT2}/Lrrc8A^{fl/fl}* mice, treated by tamoxifen from day 1 to 21, then stimulated with MSU or CPP (200 μ g/ml, 6 h, $n = 5$ and 6 independent experiments). Values are mean \pm SEM. Two-tailed unpaired t-test (**a**, **h**), two-way ANOVA, Sidak's multiple comparisons test (**b–g**, **i**).

activation of PLC-calcium pathway, eventually contributing to NLRP3 inflammasome activation and IL-1 β production.

Osmolarity changes occur in multiple physiological and pathological conditions such as cell proliferation, transepithelial transport, tissue damage, necrosis or inflammatory diseases^{27,28}. Here we reported that SF osmolarities of patients with gout (MSU) and CPP inflammatory flares are decreased as compared to patients suffering from osteoarthritis (OA). Hypotonic SF is also a characteristic of

rheumatoid arthritis, a different joint-inflammation disease also associated with high production of inflammatory cytokines^{29,30}. We observed that extracellular osmolarity modulated crystal-induced inflammation (MSU and CPP): hypertonic solution prevents MSU and CPP-mediated IL-1 β secretion. Therefore, in patients with gout and CPP inflammatory flares, both reduced SF osmolarity and crystal exposure may be responsible for inflammatory cytokines production. Our present results and those of others support that increasing



plasma osmolarity reduces the inflammatory responses encountered during gout and chondrocalcinosis flares, intracerebral hemorrhage or acute distress respiratory syndrome^{31,32}. Here, we had similar observations in rodents by using crystal-evoked inflammation in an air pouch model, and we found that crystal-induced inflammation

was reduced by artificially increasing plasma osmolarity with mannitol. The identification of this osmotherapeutic effect paves the way for the development of alternative therapeutic strategies in humans to dampen inflammation, especially in the context of microcrystal-mediated joint inflammation.

Fig. 5 | Activation of LRRC8 mediates ATP release by THP-1 macrophages. **a** ATP levels in supernatants of control and LRRC8A-KD THP-1 cells under isotonic or hypotonic solutions \pm DCPIB ($n = 6-15$ from 6 independent experiments). **b** Illustration of the PNG6 biosensor fluorescence change upon extracellular ATP binding. **c** Kinetics of ATP release evoked by hypotonic solution in control and LRRC8A-KD THP-1 cells expressing the PNG6 biosensor with/without DCPIB. Maximum fluorescence was evoked by ATP application at the end of the recordings ($n = 5$ recordings from 3 independent experiments). **d-f** ATP whole-cell currents in control THP-1 cells in isotonic and hypotonic ATP bath solutions with/without DCPIB (**d**). I/V curves (**e**) and mean currents at -100 mV (**f**) in isotonic (black) and hypotonic solution (green, 5 min) and with DCPIB (light green). $n = 6$ independent recordings. **g** Lentiviral construction expressing PNG6-P2A-Scarlet and images showing ATP release (green PNG6) and surface/volume decrease (red mScarlet) in

control THP-1 cells under hypotonic solution. Yellow and blue arrows identified cells with different time responses. Scale bar $20 \mu\text{m}$. $n = 3$ independent experiments. **h** Single-cell video recording of surface change and ATP release in control and LRRC8A-KD THP-1 cells expressing PNG6. Colored lines represent individual cells; black lines show mean surface change and ATP-evoked fluorescence. **i** Surface change (upper) and ATP release (lower) in 3 cells during a hypotonic challenge. **j** Time correlation between ATP release event and RVD induction ($n = 32$ cells from 2 independent experiments). **k** ATP levels in supernatants of control and LRRC8A-KD THP-1 cells exposed to MSU or CPP crystals with/without DCPIB. $n = 8-23$ from 8 independent experiments (control THP-1) and $n = 9-21$ from 7 independent experiments (LRRC8A-KD cells). Values are mean \pm SEM. One-way ANOVA (**f**), 2-way ANOVA, Sidak's multiple comparisons test (**a, k**). Spearman correlation test (**j**).

In our study, blocking aquaporin channels by HgCl_2 completely abolished MSU and CPP crystal-induced inflammation both in vivo and in vitro. Water influx through aquaporins has been proposed to occur following the increase of intracellular osmolarity provoked by intralysosomal dissolution of phagocytosed MSU crystals³³ and to be responsible for decreased intracellular potassium level and subsequent inflammasome activation. Similarly, aquaporin 1 was identified as contributing to silica-induced lung inflammation³⁴ and aquaporin 3 to NLRP3 inflammasome activation under various inflammatory conditions³⁵. These findings further support the implication of aquaporin and change in cell volume in microcrystal-induced inflammation.

Our data also demonstrate that in the THP-1 cell line, the knock-down of LRRC8A (the mandatory subunit of VRAC) is sufficient to reduce crystal-evoked RVD, ASC speck formation, and IL-1 β release. Moreover, conditional inactivation of LRRC8A in macrophages reduced crystal-evoked inflammation in the air pouch mouse model. Cell swelling and LRRC8 activation were previously found responsible for NLRP3 inflammasome activation on macrophage exposure to hypotonic challenge^{7,15,36}. Our results support that LRRC8-mediated NLRP3 activation is not limited to hypotonic conditions but can be triggered by crystal exposure. This observation is consistent with our previous results showing that MSU crystal-induced inflammasome activation is impaired by saline hypertonic solution in vitro⁷. Our data support that MSU and CPP crystal-activated NLRP3 inflammasome depends on LRRC8 activation and RVD initiation.

Although our results point to altered intracellular osmolarity caused by crystal exposure, we cannot exclude that crystals could activate specific intracellular pathways leading to LRRC8 activation. Nor can we exclude the involvement of additional anion channels in NLRP3 activation. For example, chloride intracellular channel proteins 1-6 (CLICs 1-6) play a major role in LPS-, ATP-, nigericin- and MSU crystal-induced IL-1 β production and NLRP3 inflammasome activation^{37,38}. Notably, genetic deletion of CLIC 1, 4, and 5 partially abolished MSU crystal-activated NLRP3 inflammasome³⁷.

MSU, silica or alum crystal exposure induced ATP and IL-1 β release in both BMDMs and THP-1 cells²⁴. From pharmacological approaches (carbenoxolone and flufenamic acid), ATP release was thought to be mediated by the connexin/pannexin pathways. Yet these drugs also affect LRRC8 activity^{10,20}. Several studies support the permeability of LRRC8 to chloride ions but also to negatively charged molecules such as glutamate, cGAMP, or glutathione^{11,39-41}. By combining several approaches, including electrophysiology and real-time extracellular ATP imaging, we show that LRRC8 channels are also permeant to ATP and that LRRC8 activation evoked by crystal exposure or hypotonic challenge results in ATP release. An osmolarity-dependent permeability to ATP was previously described in oocytes following over-expression of both LRRC8A/8E subunits⁴². Yet, ATP could be secreted by other mechanisms dependent on LRRC8 expression and activation.

We also provide evidence that LRRC8-evoked ATP release is essential to RVD and NLRP3 inflammasome activation. Implication of purinergic signaling in inflammasome activation has already been

reported. For instance, P2X7 receptor is a well-known activator of NLRP3 inflammasome in macrophages^{43,44} and the contribution of P2X and P2Y receptors in nanoparticle-induced IL-1 β release has been reported⁴⁵. Here, we observed that P2X7 receptor is not involved in MSU and CPP crystal-induced IL-1 β production as previously reported by others²⁴. Using apyrase or specific inhibitors of P2Y2 or P2Y6, we showed that impairing purinergic signaling blocked IL-1 β release induced by hypotonic challenge or crystal exposure. In the air pouch model, P2Y6 inhibition was sufficient to inhibit MSU and CPP crystal-induced IL-1 β release and reduced the inflammation score. These data are in agreement with previous studies showing that administration of MRS2578, a potent P2Y6 inhibitor, affected MSU crystal-induced neutrophil influx and activation in vivo^{46,47}. In this study, we observed that P2Y receptors acted downstream of LRRC8 activation and ATP release. Yet, P2Y2 and P2Y6 seem to act through different pathways. Indeed, P2Y2 antagonist is able to inhibit RVD in the hypotonic condition, whereas P2Y6 has no effect. Involvement of multiple purinergic receptors to crystal-evoked inflammation has already been proposed²⁴. In particular, P2Y6 inhibition blocks phagocytosis of MSU crystals by polymorphonuclear leukocytes and neutrophil extracellular trap⁴⁶. P2Y2 and P2Y6 receptors, through their coupling with Gq proteins and subsequent activation of phospholipase C (PLC), play crucial roles in calcium mobilization. An intracellular Ca^{2+} increase has been reported to be essential for the activation of the NLRP3 inflammasome by multiple stimuli^{26,48,49}. Additionally, we found that blocking the PLC pathway inhibited inflammasome activation induced by MSU and CPP crystals. While the exact mechanisms by which increased intracellular calcium leads to inflammasome activation remain to be fully elucidated, it has been proposed that calcium could directly promote NLRP3-ASC association⁵⁰, causes mitochondrial Ca^{2+} overload and mitochondrial dysfunction leading to mitochondrial reactive oxygen species (mtROS) production^{26,51,52}. In any case, P2Y2 and P2Y6 are necessary, but other key cellular events, such as K^+ and Cl^- efflux, are also required to trigger inflammasome activation in coordination with purinergic signaling and calcium mobilization.

Collectively, our findings suggest that osmotherapy targeting the LRRC8 channels or directly inhibiting this osmo-sensitive channels could represent innovative therapeutic strategies to dampen microcrystal-related inflammation.

Methods

Ethics statement, quantification of osmolarity, IL-1 β content in patient synovial fluid

Synovial fluid (SF) was collected from patients during the management of gout, CPP deposition disease flares and osteoarthritis joint effusion. Patients gave written informed consent for use of these waste samples for research. Ethical approval was obtained from the French national ethical committee *Comité de protection des personnes participant à la recherche* (DC 2020-3976). Gout and CPP deposition diagnoses were established by the identification of MSU and CPP crystals, respectively, on SF analysis by compensated polarized microscopy. Osteoarthritis diagnosis was based on clinical and plain radiography signs. We

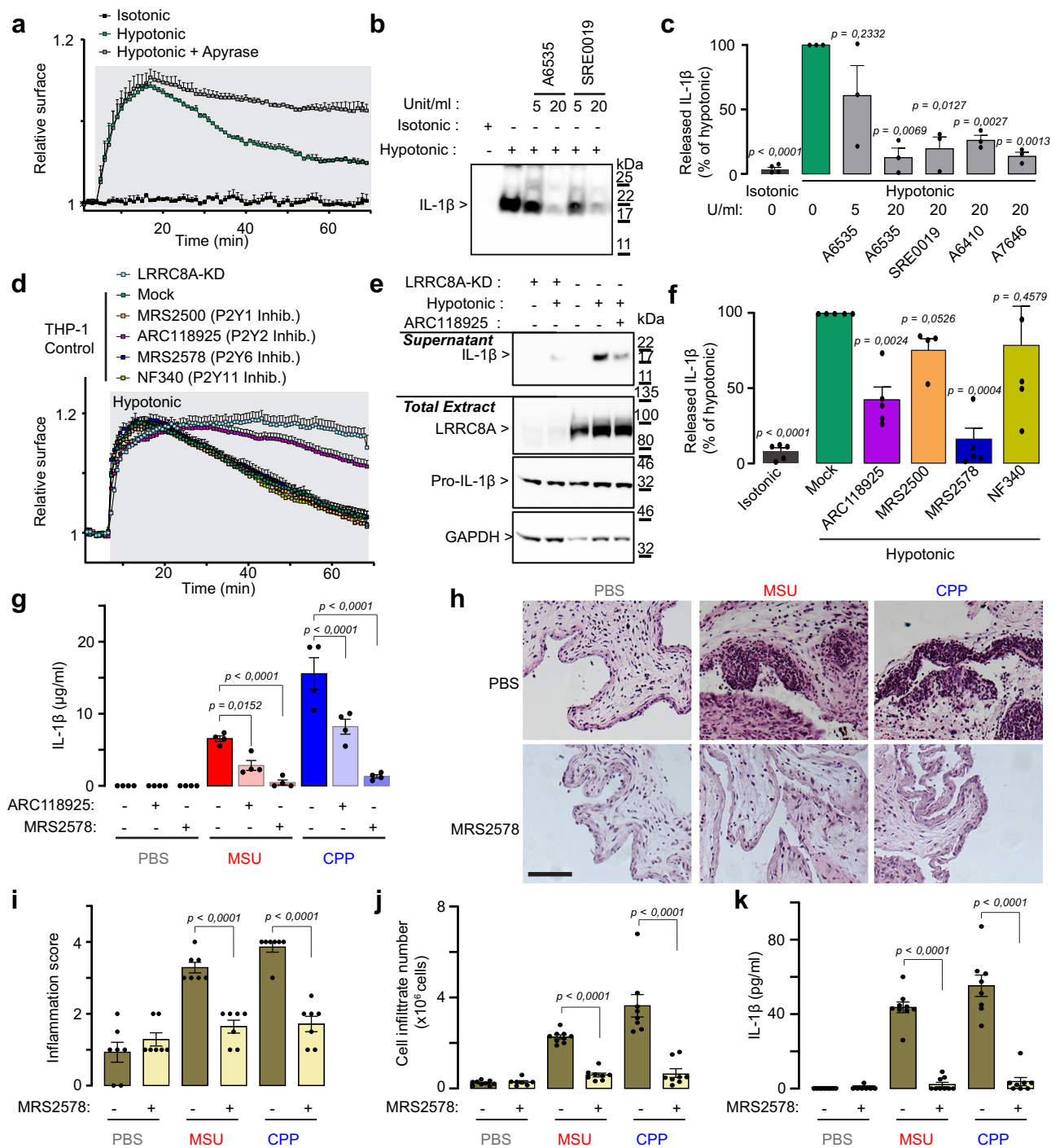


Fig. 6 | LRRC8-evoked ATP release governs regulatory volume change and NLRP3 inflammasome activation via P2YR signaling. **a** Monitored surface changes (mScarlet fluorescence) in control THP-1 cells under hypotonic conditions (100 mOsm.l⁻¹) with and without apyrase (A6535, 20U/ml). *n* = 3 independent experiments with 30–66 cells per experiment. **b, c** Western blot analysis and quantification of IL-1 β release in control THP-1 cells under hypotonic conditions with varying apyrase levels and grades. Values normalized to the hypotonic condition without apyrase, mean \pm SEM from 3–5 experiments. **d** Surface changes in control and LRRC8A-KD THP-1 cells during hypotonic challenge with various P2Y receptor antagonists (10 μ M). *n* = 3 independent experiments with 30–66 cells per experiment. **e** Western blot analysis of mature IL-1 β in supernatants and pro-IL-1 β and LRRC8A expression in cell extracts from control and LRRC8A-KD cells under hypotonic conditions with/without P2Y2 antagonist ARCI18925 (10 μ M).

f Quantification of IL-1 β release in control THP-1 cells under hypotonic stimulation with/without 10 μ M of each antagonist ARCI18925 (P2Y2), MRS2500 (P2Y1), MRS2578 (P2Y6), or NF340 (P2Y11). Results normalized to conditions without antagonists, *n* = 4–5 independent experiments. **g** ELISA measurement of IL-1 β levels in the supernatant of control THP-1 cells exposed to MSU or CPP crystals (200 μ g/ml, 3 h) with/without antagonists ARCI18925 (10 μ M) or MRS2578 (10 μ M). *n* = 4 independent experiments. **h, i** Micrographs and inflammation scores for air pouch membranes from control and MRS2578-treated mice injected with PBS, MSU, or CPP crystal (*n* = 8 mice/group). Scale bar, 40 μ m. **j, k** Cell infiltration (**j**, *n* = 9 PBS and MSU, 8 CPP, 7 MRS, 8 MRS + MSU/ CPP) and IL-1 β (**k**, *n* = 9 PBS and MSU, 8 CPP, 7 MRS, 9/8 MRS + MSU/ CPP) levels in air pouch lavage from mice treated with/without MRS2578. Values are mean \pm SEM. Two-tailed unpaired t-test (**c, f**), two-way ANOVA, Sidak’s multiple comparisons test (**g, i–k**).

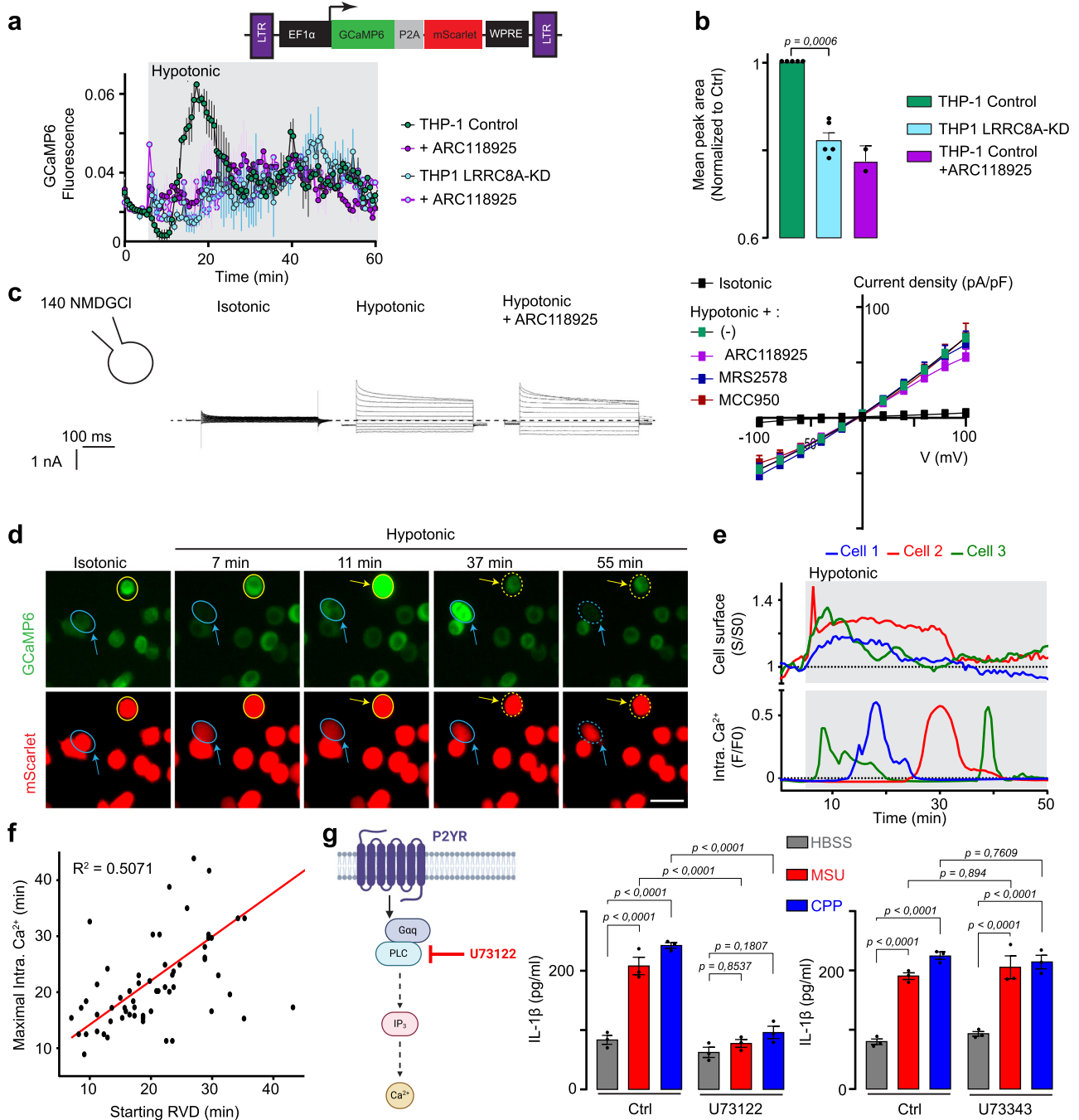


Fig. 7 | Intracellular calcium signaling through P2YR is required for NLRP3 inflammasome activation. **a** Video-microscopy recording of intracellular calcium during hypotonic challenge in control and LRRC8A-KD THP-1 cells expressing GCaMP6-P2A-mScarlet, with or without P2Y2 antagonist ARC118925 (10 μ M). **b** Quantification from **(a)** showing area under the peaks averaged and normalized to control. Data are mean \pm SEM from $n = 5$ experiments for control and LRRC8A-KD, $n = 2$ experiments for ARC118925. 30–60 cells per experiment. **c** Chloride currents in control THP-1 cells in isotonic (300 mOsm.l-1) and hypotonic (220 mOsm.l-1) NMDGCl solutions, with/without ARC118925 (10 μ M). I/V curves show mean current density under hypotonic conditions with ARC118925, MRS2578, or MCC950 (10 μ M). Pipette solution contained NMDGCl. Data are mean \pm SEM from 4 to 15 cells, $n = 4$ –15 experiments. **d–f** Simultaneous intracellular calcium signals and cell surface analysis during hypotonic challenge at single-cell level.

d Combined recording of cell surface variation (mScarlet) and intracellular calcium (GCaMP6). Scale bar 20 μ m. **e** Single-cell analysis shows RVD initiation coincides with a burst of intracellular calcium release. **f** Time correlation between RVD initiation and peak of intracellular calcium signal. **d–f**: $n = 2$ experiments, analysis of 70 cells. **g** Left panel: cartoon of PLC pathway activation by Gq-coupled P2YR leading to intracellular calcium mobilization. Middle and right panels: ELISA results of IL-1 β levels in supernatants of control THP-1 cells exposed to MSU or CPP crystals (200 μ g/ml, 4 h) with/without PLC inhibitor (U73122, 5 μ M) or its inactive analog (U73343, 5 μ M). $n = 3$ independent experiments. Values are mean \pm SEM. Two Way ANOVA with Tukey’s multiple comparison post hoc test. Panel **g** Created with BioRender.com released under a Creative Commons Attribution-NonCommercial-NoDerivs 4.0 International license <https://creativecommons.org/licenses/by-nc-nd/4.0/deed.en>.

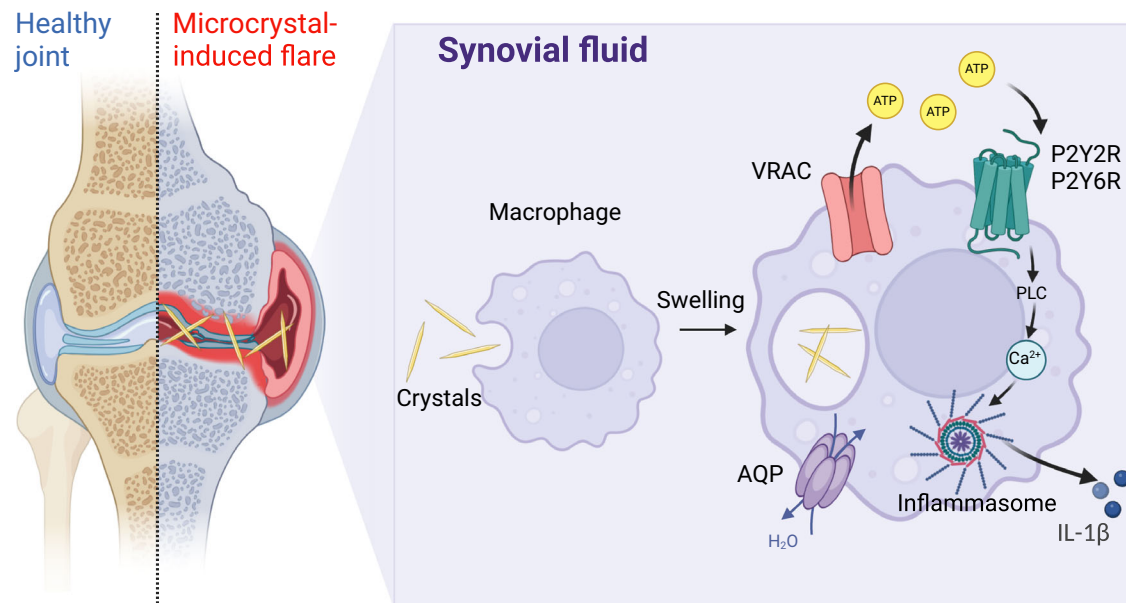


Fig. 8 | Signaling pathways involved in micro-crystallin joint inflammation. Scheme illustrating that microcrystal-induced production of proinflammatory cytokine IL-1 β relies on cell volume regulation. During microcrystal-induced inflammation, both the decrease of synovial fluid osmolarity and the presence of microcrystals induce resident macrophage swelling, which activates the volume regulatory anion channels LRRC8 leading to ATP outflow. ATP in an autocrine and/

or paracrine way activates purinergic P2Y2 and P2Y6 receptors that, through a PLC and intracellular calcium-dependent pathways contribute to NLRP3 activation and subsequent pro-IL-1 β maturation and release. Created with BioRender.com released under a Creative Commons Attribution-NonCommercial-NoDerivs 4.0 International license <https://creativecommons.org/licenses/by-nc-nd/4.0/deed.en>.

separated inflammatory SF related to microcrystal flare (defined by cell concentration > 2000/mm³ and presence of crystals detected by polarized light microscopy) from mechanical OA synovial fluids (defined by cell concentration <1000/mm³) and we excluded mechanical SFs containing CPP crystals detected by polarized light microscopy. Cell count was performed manually with a Malassez cell counting chamber. When cell count exceeded 500/mm³, May-Grunwald-Giemsa staining was performed, and the cells were classified as erythrocytes, neutrophils, lymphocytes and other types.

SF from patients were centrifuged to eliminate cells, crystals and debris. Supernatants were collected and stored at -80 °C. Osmolarities of the centrifugated SF or of cell culture media were measured by using the freezing point technique (Roebing Osmometer automatik) and IL-1 β concentration was quantified with an ELISA commercial kit (Invitrogen).

Ethics statement and mouse air pouch model

This study was approved by the French national ethical committee *Le comité d'éthique en expérimentation animale Lariboisière/Villemin n°9* (APAFIS#28637). Mouse studies were carried out in accordance with European Union directives (2010/63/UE) and French ethical laws guidelines (act no. R214; 87-137; *Ministère de l'Agriculture*) and followed the ARRIVE guidelines (Animal Research: Reporting of In vivo Experiments; <http://www.nc3rs.org.uk>). Each animal was humanely handled throughout the experiment in accordance with internationally accepted ethical principles for laboratory animal use and care, and all efforts were made to minimize animal suffering.

Male 8-week-old wild-type (WT) C57Bl/6J mice were provided by the Janvier Lab. An air pouch was created by dorsal subcutaneous injections of 3 ml sterile air on days 0 and 3. On day 6, crystals (MSU or CPP, 1 mg/ml, 1 ml) or phosphate buffered saline (PBS) (1 ml) were injected into the air pouch. To artificially increase plasma osmolarity, we used intraperitoneal (IP) injection of mannitol 20 % (1 ml) for 3 consecutive days before crystal injection. To inhibit aquaporin channels, we treated mice with 10 μ g/g mercury chloride (HgCl₂; Sigma) by IP injection 30 min before crystal stimulation. Untreated mice received an IP injection of the same volume of saline (PBS). Inflammation was

studied 6 h after crystal or PBS stimulation, assessing in air pouch lavages the concentration of inflammatory mediators by using an ELISA commercial kit (IL-1 β , Invitrogen) and cell infiltration by manual counting (absolute number) and FACS analysis (quantification of the proportion of neutrophils and macrophages). Air pouch membranes were collected and fixed with paraformaldehyde (PFA) 4%. Tissue inflammation was histologically estimated on collected membranes after paraffin embedding and hematoxylin-eosin (HE) staining by using a semi-quantitative score¹⁶.

Conditional deletion of *Lrrc8A* in monocyte/macrophage lineage in vivo

Male 8-week-old *Cx3cr1CreERT2/Lrrc8A^{fllox/flox}* C57Bl/6J mice (kind gift from Pr. T Jentsch) and their control *Cx3cr1CreERT2* C57Bl/6J mice underwent IP injection of 6-OH-tamoxifen (0.1 mg/g, Sigma T5648) for 5 consecutive days to specifically inactivate the *Lrrc8A* gene in the monocyte/macrophage lineage and were called *Lrrc8^{ΔMo}* and *Lrrc8^{cont}* mice, respectively. One day after tamoxifen treatment, the inflammation induced by crystals was assessed with the air pouch model. Deletion of *Lrrc8A* was controlled by FACS analysis with macrophages isolated from air pouch lavage and bone marrow-derived macrophages (BMDMs).

Histology

To measure the inflammatory infiltrate, mouse air pouches were fixed in PFA 4%, embedded in paraffin, and serial 5 μ m-thick sections were obtained. Sections were then stained with HE. Inflammation was assessed with a semi-quantitative score as we previously described¹⁶. In brief, the inflammatory score of each membrane was the highest score observed in 10 random sections.

THP-1 cell culture, transduction and differentiation

THP-1 cells were maintained in suspension culture in RPMI 1640 medium (Invitrogen), 10% fetal bovine serum (FBS, Thermo Fisher) and 1% penicillin-streptomycin (PS, 10000 U/mL, Thermo Fisher). Cells were grown in a humidified atmosphere of 95% air/ 5% CO₂ at 37 °C in a cell culture incubator. Cells were split 1/10 every 3 to 4 days, then cells

at 50% confluence were plated (1 million cells) in a 6-well plate 24 h before lentiviral transduction and transduced with 6 μ L virus encoding the PNG6-P2A-Scarlet biosensor²⁵ or GCamp6-P2A-Scarlet mixed with 6 μ L LentiBlast solution (3 μ L LentiBlast A solution and 3 μ L LentiBlast B solution, Ozbiosciences). Lentiviral production was previously described²⁵. One week after transduction, most cells stably expressed the transgene and were cultivated in RPMI 1640 + 10 % FBS + 1 % PS. Differentiation of THP-1 cells in macrophages involved 40-min incubation in media supplemented with phorbol 12-myristate 13-acetate (PMA) 200 nM (Sigma). Treated cells were then seeded in 96-well plates (140,000 cells/well) until imaging experiments, 24 h later for time lapse imaging or 48 h later for plate reader experiments.

For experiments related to cytokine quantification in the supernatant, primed THP-1 cells were seeded in 24-well dishes at 300,000 cells/well and left overnight in complete media. Then, cells were stimulated with sterile MSU or mCPP crystals (200 μ g/ml) in isotonic serum-free media (PBS, 300 mOsm.l⁻¹), or hypertonic solution (addition of 100 mM Mannitol, 400 mOsm.l⁻¹) for 3 h, or with hypotonic solution (dilution 1/3 with water, 100 mOsm.l⁻¹) for 60 min as described⁷. For some experiments, THP-1 cells were pre-incubated with HgCl₂ (Sigma M1132), 4-(2-Butyl-6,7-dichloro-2-cyclopentyl-indan-1-on-5-yl) oxobutyric acid (DCPIB; Tocris 82749-70-0), U73122 (Tocris 1268), U73343 (Tocris 4133) and D-mannitol (Sigma, M9647) 30 min before stimulation. Cell culture supernatants were collected and stored at -20 °C until cytokine quantification.

THP-1 knock-down cells (LRRC8A-KD) were generated with lentiviral shRNA (TRCN0000118623 from Sigma, Sequence: CCGGCCG CAACAAGATCGAGAAGATCTCGAGATCTTCTCGATCTTGTTCGGGTTT TTG) and were selected by culturing cells in the presence of puromycin (3 μ g/ml) for 7 days.

BMDM isolation, culture and differentiation

Bone-marrow cells were recovered from tibia and femoral bones of 8-week-old mice (WT, homozygous *Cx3cr1CreERT2* and *Cx3cr1CreERT2/Lrrc8A^{fllox/fllox}*^{22,23} and cultured in 24-well plates at 2 million cells/ml in 10%-L929 conditioned RPMI1640 media supplemented with 10% FBS, HEPES (5 mM), L-glutamine (2 mM), penicillin (100 U/ml), and streptomycin (100 μ g/ml) until complete differentiation of BMDMs. To delete *Lrrc8A* expression, bone-marrow cells isolated from *Cx3cr1CreERT2* and *Cx3cr1CreERT2/Lrrc8A^{fllox/fllox}* mice were treated with tamoxifen (Sigma, H7904) on days 1, 3, 4, 7, and 11 and cultured for 21 days. BMDMs were primed overnight with ultrapure lipopolysaccharide (LPS; 20 ng/ml) before stimulation with microcrystals or PBS in serum-free media for 6 h. Supernatants were collected and frozen at -20 °C until cytokine quantification.

Monosodium urate (MSU) and calcium pyrophosphate (CPP) crystals

MSU and monoclinic CPP crystals were synthesized, characterized and sterilized as described¹⁶. MSU and mCPP crystal specific surface were 1.4 \pm 0.1 m²/g and 2.8 \pm 0.1 m²/g, respectively. Both mCPP and MSU were needle-like crystals, and their average length/width were 16.0/1.5 μ m and 32.5/2.9 μ m, respectively.

Cytokine quantification

Cytokine production in supernatants or air pouch lavage was measured by using ELISA kits for IL-1 β , IL-8 and tumor necrosis factor α (TNF) (Invitrogen, Thermo Fisher).

Quantification of NF-KB activation THP-1-Lucia

THP-1 cells containing an NF- κ B-inducible Luc reporter construct (THP-1-Lucia NF- κ B cells, Invivogen) were used to assess NF- κ B activation. THP-1-Lucia cells were cultured in RPMI 1640 media supplemented with pyruvate 1 mM (Gibco) and the selection antibiotic zeocin (Invivogen).

PMA-primed THP-1-Lucia cells were washed twice and stimulated for 8 h with MSU or CPP crystals (200 μ g/ml) or heat-killed *Listeria monocytogenes* (HKLM, Invivogen: positive control of NF- κ B induction) in serum-free medium. Absolute luciferase activity was determined in the supernatants with a Xenius luminometer (SAFAS Monaco) according to the manufacturer's instructions.

Flow cytometry

A total of 0.1 million cells from air pouch lavages were stained with anti-F4/80-APC (clone REA126; Miltenyi Biotechnology) and anti-Ly6G-PE mouse monoclonal antibodies for 20 min at 4 °C, washed in PBS, and analyzed with the BD FACS Canto II cytometer (BD Bioscience).

Anti-LRRC8A antibody (Sigma SAB2108060) was used to stain 0.1 million pouch infiltrate cells and BMDMs incubated overnight at 1/1000 dilution to determine the efficiency of the knockdown. The expression of LRRC8A was analyzed the following day for 60 min by using a rabbit secondary antibody conjugated to FITC. Data were analyzed by using BDFACS Diva software (BD Biosciences).

Electrophysiological studies

The ruptured whole-cell configuration of the patch-clamp technique was used to assess the chloride and adenosine triphosphate (ATP) current permeabilities of the LRRC8/VRAC. Cell currents and cell capacitances were recorded by using an EPC 10 amplifier (HEKA Elektronik, Germany). Cells were held at -40 mV, and 400-ms pulses from -100 to +100 mV were applied in 20-mV increments. The offset potentials between both electrodes were zeroed before sealing and corrected for liquid junction potentials as described⁵³. Original whole-cell traces were depicted after use of a 3-kHz Bessel filter. Currents were measured 10 ms after the onset pulse, and I/V curves were corrected by the capacitance of the cells (pA/pF, current density). Patch pipettes (3-4 MOhm resistance) were created from borosilicate capillary tubes (1.5-mm OD, 1.1-mm ID, Vitrex, Denmark) by using a two-stage vertical puller (model PP 830, Narishige, Japan).

For chloride current recordings, the pipette solution contained (in mM) 140 NMDGCl, 10 HEPES (pH 7.4, HCl), 5 EGTA and 5 MgATP (-290 mOsm.l⁻¹). For ATP current recordings, the pipette solution contained (in mM) 100 Na₂ATP, 5 MgATP, 5 HEPES (pH 7.4, NaOH) and 5 EGTA (-290 mOsm.l⁻¹).

The normal NMDGCl bath solution contained (in mM) 120 NMDGCl, 10 HEPES (pH 7.4, HCl), 1 CaCl₂, 1 MgCl₂, 80 mannitol (300-310 mOsm.l⁻¹). The normal ATP bath solution contained (in mM) 100 Na₂ATP, 5 HEPES (pH 7.4, NaOH), 70 mannitol (320-330 mOsm.l⁻¹). This bath isotonic solution was designed to avoid spontaneous activation of LRRC8/VRAC currents. Hypotonic NMDGCl solution (220 mOsm.l⁻¹) or Na₂ATP (260 mOsm.l⁻¹) solution was obtained by removing the mannitol from the normal NMDGCl or ATP bath solution.

Measurements of cell volume change with the calcein self-quenching method

Measurements of changes in cell volume in THP-1 cells or BMDMs involved the calcein fluorescence self-quenching method. Briefly, calcein at high concentration undergoes spontaneous self-quenching, and its fluorescence intensity decreases with increasing intracellular calcein concentration, which fluctuates according to cell volume variations^{20,54}. Macrophages were cultured on poly-lysine-coated 24-well plates for 2 days. Cells were then loaded for 40 min with a solution calcein-AM (Sigma-Aldrich). Cells were then washed 3 times and incubated with an isotonic medium containing (in mM) 145 NaCl, 5 KCl, 1 MgCl₂, 0.4 CaCl₂, 10 glucose, and 10 HEPES, pH 7.4 (300 mOsm.l⁻¹). After a baseline recording period (10 min), the medium was replaced with hypotonic bath solution (100 mOsm.l⁻¹) or isotonic solution containing MSU or CPP crystals (200 μ g/ml). The fluorescence was measured every 60 or 90 s for 120 min by using a plate reader (Ex: 460 nm, Em: 520 nm; Synergy HT, Biotek). Values (representing the cell volume) were

normalized to the fluorescence measured at the beginning of the experiment (first 10 min) in isotonic bath solution (F/F₀).

Western blot analysis

Cells were washed with PBS and scraped in lysis buffer (20 mM HEPES [pH 7.4], 100 mM NaCl, 5 mM EDTA, 1% TX-100) supplemented with a mixture of protease and phosphatase inhibitors (Thermo Fisher). After 30 min at 4 °C, lysates were centrifuged (15,900 × *g*, 10 min, 4 °C) and the supernatant was collected and mixed with Sample Buffer (NuPAGE, Thermo Fisher). Cell supernatants were clarified by brief centrifugation, concentrated by using 10-kDa nominal molecular mass cutoff filters (Millipore), then mixed with Sample Buffer, as described above. Proteins were separated on 4–12% Bis-Tris gels (NuPage Novex, Thermo Fisher) and transferred to nitrocellulose membranes (iBlot2, Thermo Fisher). Proteins were detected by using the primary antibodies for IL-1 β (Santa Cruz Biotechnology, sc-7884); LRRc8A (Sigma, HPA016811); Apoptosis-associated Speck-like protein containing a caspase activation and recruitment domain (CARD) (ASC; Santa Cruz Biotechnology, sc-22514-R); NLRP3 (Adipogen, AG-20B-0014); tubulin (DSHB clone 12G10); and GAPDH (Cell Signaling, 3683), all diluted at 1/1000, and appropriate HRP-coupled secondary antibodies and Clarity Western ECL substrate (Biorad).

Immunolabelling of ASC speck

A total of 250,000 PMA-primed control and LRRc8A-KD THP-1 cells were plated on glass coverslips; cells were preincubated with PBS, HgCl₂ or DCPIB and stimulated with crystals for 3 h or hypotonic solutions for 1 h, then fixed in 4% PFA. The membrane was permeabilized (5 min at room temperature, 0.1% Triton X-100 in PBS), washed 3 times, incubated overnight at 4 °C with ASC antibody (1/200, Santa Cruz Biotechnology, sci22514-R), then revealed with DyLight-550-conjugated anti-IgG secondary antibody (Pierce). DAPI was used as a counterstain for nuclei. ASC speck formation was analysed by confocal microscopy with a 63x magnification lens or an Apotome and 40x magnification lens.

Plate reader imaging for ATP extracellular measurement

At 48 h after differentiation, primed THP-1 cells expressing PNG6 biosensor were seeded in 96-well plates, washed and incubated for 20 min in Flex buffer (HBSS (Thermo Fisher) supplemented with 20 mM HEPES, pH 7.4, 1 mM MgSO₄, 3 mM Na₂CO₃, and 0.4 mM CaCl₂) at 37 °C. For hypotonicity experiments, H₂O Milli-Q water + 0.4 mM CaCl₂ were added to the well to obtain 160 mOsm.l⁻¹ solutions. The osmotic concentration of each solution was verified by using an osmometer. For pharmacological experiments, cells were preincubated for 15 min with drugs diluted in FLEX buffer. Fluorescence (λ exc/em 485/540) was acquired with an INFINITY 500 (TECAN) plate reader. The recording was performed at 0.15 Hz. All experiments were performed at 37 °C.

Time-lapse imaging

Primed THP-1 cells seeded in 96-well plate were imaged 24 h after differentiation. At this time, the shape of macrophages is round and allows for automatic detection of the cell surface. THP-1 cells were washed and incubated for 20 min in Flex buffer (HBSS supplemented with 20 mM HEPES, pH 7.4, 1 mM MgSO₄, 3 mM Na₂CO₃ and 0.4 mM CaCl₂) at 37 °C. For hypotonicity experiments, H₂O Milli-Q water + 0.4 mM CaCl₂ was added to the well to obtain 100 mOsm solutions. The osmotic concentration of each solution was verified by using an osmometer. For pharmacological experiments, cells were pre-incubated for 15 min with drugs diluted in FLEX buffer. All cells were imaged by using a motorized inverted epifluorescence microscope (ZEISS AXIO OBSERVER 7) equipped with an incubator (5% CO₂, 37 °C) and a CMOS Hamamatsu ORCA camera controlled via ZEN software. Acquisitions involved using a 20X objective lens at 2 frames/min (λ exc/em 485/540, 530/590). For image analysis, an automatic ROI-based analysis was developed on

IMARIS that allowed for simultaneously detecting GCaMP6s signals (λ exc/em 485/540) and cell surface (λ exc/em 530/590).

RT-qPCR analysis in BMDMs

RNA from BMDMs was extracted by using the Qiagen RNeasy Plus Mini kit (Qiagen, #74136) following the manufacturer's protocol. Total RNA quality was checked by using the 2100 Bioanalyzer (Agilent); All RNAs had RNA Integrity Numbers (RINs) > 8.0. Reverse transcription of total RNA involved using the iScript kit (BioRad). Quantitative PCR was performed in 384-well plates in a final volume of 10 μ l by using SYBR Green dye detection on the LightCycler480 system (Roche-Diagnostic).

Primer sequences were designed by using Primer Express software (Thermo Fisher) or Primer-3⁵⁵ and tested for specificity and efficiency (LightCycler 480, Roche). Expression of selected mouse genes was quantified by the comparative - Δ Ct method using Cox6b1 as a normalizing gene. In shRNA-mediated knockdown experiments, gene expression was further normalized to that of control virus-treated cultures and expressed as - $\Delta\Delta$ Ct. Primer sequences were as follows:

Lrrc8a: s- GGGTGAACCATGATTCCGGTGAC as- GAAGACGGCA ATCATCAGCATGAC

Lrrc8b: s- ACCTGGATGGCCACAGGTAATAG as- ATGCTGGTCA ACTGGAACCTCTGC

Lrrc8c: s- ACAAGCCATGAGCAGCGAC as- GGAATCATGTTTCTCC GGGC

Lrrc8d: s- ATGAGGAGTGAAGTCTCCTGTCTCG as- CTTCCGCAA GGGTAAACATTCTCTG

Lrrc8e: s- ACCGTGGCCATGCTCATGATTG as- ATCTTGTCTCTGT GTCACCTGGAG

Cfr: s- GCAGCCTTACTTTGAAACTC as- AACAGCAATGAAGAA GATGAC

Tmem16a: s- GGCATATTCCAGAGGAGTCAA as- TCCATGTCTAG CTTCACTTTGTC

Tmem16b: s- GCCAGGGATCCATCTTTGT as- CCTGCTTTGATCT CGTACATTTT

Tmem16c: s- GCAGAGAGGCTGAATATCAGGA as- GCATCCTGCC CATTGATT

Tmem16d: s- TGACTGGGATTTGATAGACTGG as- GCTTCAAAC TGGGGTCTGTAT

Tmem16e: s- TGGAAACATTAAGAAGCCATTT as- GAGTTTGT CCGAGCTTTTCG

Tmem16f: s- AGGAATGTTTTGCTACAAATGGA as- GTCCAAGG TTTTCCAACACG

Tmem16g: s- GCTCTGTGGTGATCGTGGT as- GGCACGGTACA GGATGATAGA

Tmem16h: s- GGAGGACCAGCCAATCATC as- TGCTCGTGGACAG GGAAC

Tmem16j: s- CGGAAGTCAGGTAGGAGCAC as- ATCCGGAGGC TCTCTTCG

Tmem16k s- TTGTATCCAGGAAATCATTGTTG as- AAGCTTCTTC AGGGCTTCACT

Cox6b1: s- CTCCGGGACAATCTTTAGGA as-GGGGGCAGTTTTGT AGTTCTT.

Quantification of ATP release in supernatant

WT and LRRc8A-KD THP-1 cells were cultured for 24-48 h after PMA priming. Culture medium was replaced with a isotonic bath solution for 1 h and cells were exposed to isotonic solutions (PBS-like containing 138 mM NaCl, 2.7 mM KCl, 1.4 mM KH₂PO₄, 8 mM Na₂HPO₄, 10 mM HEPES, 2 mM MgCl₂, 0.4 mM CaCl₂, Pos -300 mOsm.l⁻¹), hypotonic solutions (46 mM NaCl, 2.7 mM KCl, 0.5 mM KH₂PO₄, 3 mM Na₂HPO₄, 10 mM HEPES, 2 mM MgCl₂, 0.4 mM CaCl₂, Pos -100 mOsm.l⁻¹) or isotonic solutions containing MSU or CPP crystals (200 μ g/ml) in the presence or absence of different inhibitors. Supernatants were collected at the end of the experiments (4 °C), centrifuged (10 min, 300 g), and ATP content was evaluated by using luciferine/luciferase

ATP assays (ATPlite; PerkinElmer, Waltham, MA) according to the manufacturer's instructions. The luminescence (LUM) was measured on a microplate reader (Synergy HT, BioTek, US). Values of ATP levels measured in the supernatant were normalized to protein content of each individual cultures by using DC Bio-Rad protein assays.

Data analysis

Graphics and data analysis involved using GraphPad Prism 7.0. Quantitative data are presented as mean \pm SEM. After verification of Gaussian distribution and homogenous variance of each group, two-tailed unpaired *t* test was used to compare two experimental conditions or one-way and two-way ANOVA with Sidak's multiple comparisons test to compare more than 2 experimental conditions involving 1 or 2 independent variables. For parametric or non-parametric tests, linear correlation was determined by the non-parametric Spearman test. The significance level was set at $p < 0.05$.

Reporting summary

Further information on research design is available in the Nature Portfolio Reporting Summary linked to this article.

Data availability

All data supporting the findings of this study are available in the article and its supplementary files or from the corresponding authors on request. Source data are provided with this paper.

References

1. Dalbeth, N., Gosling, A. L., Gaffo, A. & Abhishek, A. Gout. *Lancet* **397**, 1843–1855 (2021).
2. Doherty, M. et al. Efficacy and cost-effectiveness of nurse-led care involving education and engagement of patients and a treat-to-target urate-lowering strategy versus usual care for gout: a randomised controlled trial. *Lancet* **392**, 1403–1412 (2018).
3. Latourte, A. et al. Tocilizumab in symptomatic calcium pyrophosphate deposition disease: a pilot study. *Ann. Rheum. Dis.* **79**, 1126–1128 (2020).
4. Martin, W. J., Walton, M. & Harper, J. Resident macrophages initiating and driving inflammation in a monosodium urate monohydrate crystal-induced murine peritoneal model of acute gout. *Arthritis Rheumatism* **60**, 281–289 (2009).
5. Martinon, F., Pétrilli, V., Mayor, A., Tardivel, A. & Tschopp, J. Gout-associated uric acid crystals activate the NALP3 inflammasome. *Nature* **440**, 237–241 (2006).
6. Broz, P. & Dixit, V. M. Inflammasomes: mechanism of assembly, regulation and signalling. *Nat. Rev. Immunol.* **16**, 407–420 (2016).
7. Compan, V. et al. Cell volume regulation modulates NLRP3 inflammasome activation. *Immunity* **37**, 487–500 (2012).
8. Ip, W. K. E. & Medzhitov, R. Macrophages monitor tissue osmolarity and induce inflammatory response through NLRP3 and NLRC4 inflammasome activation. *Nat. Commun.* **6**, 6931 (2015).
9. Qiu, Z. et al. SWELL1, a plasma membrane protein, is an essential component of volume-regulated anion channel. *Cell* **157**, 447–458 (2014).
10. Voss, F. K. et al. Identification of LRRC8 heteromers as an essential component of the volume-regulated anion channel VRAC. *Science* **344**, 634–638 (2014).
11. Lutter, D., Ullrich, F., Lueck, J. C., Kempa, S. & Jentsch, T. J. Selective transport of neurotransmitters and modulators by distinct volume-regulated LRRC8 anion channels. *J. Cell Sci.* **130**, 1122–1133 (2017).
12. Syeda, R. et al. LRRC8 proteins form volume-regulated anion channels that sense ionic strength. *Cell* **164**, 499–511 (2016).
13. Takahashi, H., Yamada, T., Denton, J. S., Strange, K. & Karakas, E. Cryo-EM structures of an LRRC8 chimera with native functional properties reveal heptameric assembly. *Elife* **12**, e82431 (2023).
14. Liu, H. et al. Structural insights into anion selectivity and activation mechanism of LRRC8 volume-regulated anion channels. *Cell Rep.* **42**, 112926 (2023).
15. Green, J. P. et al. LRRC8A is essential for hypotonicity-, but not for DAMP-induced NLRP3 inflammasome activation. *Elife* **9**, e59704 (2020).
16. Renaudin, F. et al. Gout and pseudo-gout-related crystals promote GLUT1-mediated glycolysis that governs NLRP3 and interleukin-1 β activation on macrophages. *Ann. Rheum. Dis.* **79**, 1506–1514 (2020).
17. Edwards, J. C., Sedgwick, A. D. & Willoughby, D. A. The formation of a structure with the features of synovial lining by subcutaneous injection of air: an in vivo tissue culture system. *J. Pathol.* **134**, 147–156 (1981).
18. Campillo-Gimenez, L. et al. Inflammatory potential of four different phases of calcium pyrophosphate relies on NF- κ B Activation and MAPK Pathways. *Front Immunol.* **9**, 2248 (2018).
19. Savage, D. F. & Stroud, R. M. Structural basis of aquaporin inhibition by mercury. *J. Mol. Biol.* **368**, 607–617 (2007).
20. Friard, J. et al. Comparative effects of chloride channel inhibitors on LRRC8/VRAC-mediated chloride conductance. *Front. Pharmacol.* **8**, 328 (2017).
21. Decher, N. et al. DCPIB is a novel selective blocker of I(Cl,swell) and prevents swelling-induced shortening of guinea-pig atrial action potential duration. *Br. J. Pharm.* **134**, 1467–1479 (2001).
22. Lück, J. C., Puchkov, D., Ullrich, F. & Jentsch, T. J. LRRC8/VRAC anion channels are required for late stages of spermatid development in mice. *J. Biol. Chem.* **293**, 11796–11808 (2018).
23. Stuhlmann, T., Planells-Cases, R. & Jentsch, T. J. LRRC8/VRAC anion channels enhance β -cell glucose sensing and insulin secretion. *Nat. Commun.* **9**, 1974 (2018).
24. Riteau, N. et al. ATP release and purinergic signaling: a common pathway for particle-mediated inflammasome activation. *Cell Death Dis.* **3**, e403 (2012).
25. Ollivier, M. et al. P2X-GCaMPs as versatile tools for imaging extracellular ATP signaling. *eNeuro* **8**, ENEURO.0185-20.2020 (2021).
26. Murakami, T. et al. Critical role for calcium mobilization in activation of the NLRP3 inflammasome. *Proc. Natl Acad. Sci.* **109**, 11282–11287 (2012).
27. Hoffmann, E. K., Lambert, I. H. & Pedersen, S. F. Physiology of cell volume regulation in vertebrates. *Physiol. Rev.* **89**, 193–277 (2009).
28. Jentsch, T. J. VRACs and other ion channels and transporters in the regulation of cell volume and beyond. *Nat. Rev. Mol. Cell Biol.* **17**, 293–307 (2016).
29. Shanfield, S., Campbell, P., Baumgarten, M., Bloebaum, R. & Sarmiento, A. Synovial fluid osmolality in osteoarthritis and rheumatoid arthritis. *Clin. Orthop. Relat. Res.* **235**, 289–295 (1988).
30. Bertram, K. L. & Krawetz, R. J. Osmolarity regulates chondrogenic differentiation potential of synovial fluid derived mesenchymal progenitor cells. *Biochem Biophys. Res Commun.* **422**, 455–461 (2012).
31. Petroni, R. C. et al. Hypertonic saline (NaCl 7.5%) reduces lps-induced acute lung injury in rats. *Inflammation* **38**, 2026–2035 (2015).
32. Schreiber, D. L. et al. Mannitol and hypertonic saline reduce swelling and modulate inflammatory markers in a rat model of intracerebral hemorrhage. *Neurocrit Care* **29**, 253–263 (2018).
33. Schorn, C. et al. Sodium overload and water influx activate the NALP3 inflammasome. *J. Biol. Chem.* **286**, 35–41 (2011).
34. Rabolli, V. et al. Critical role of aquaporins in interleukin 1 β (IL-1 β)-induced inflammation. *J. Biol. Chem.* **289**, 13937–13947 (2014).
35. da Silva, I. V. et al. Aquaporin-3 is involved in NLRP3-inflammasome activation contributing to the setting of inflammatory response. *Cell Mol. Life Sci.* **78**, 3073–3085 (2021).
36. Burow, P., Klapperstück, M. & Markwardt, F. Activation of ATP secretion via volume-regulated anion channels by sphingosine-1-phosphate in RAW macrophages. *Pflug. Arch.* **467**, 1215–1226 (2015).

37. Tang, T. et al. CLICs-dependent chloride efflux is an essential and proximal upstream event for NLRP3 inflammasome activation. *Nat. Commun.* **8**, 202 (2017).
38. Domingo-Fernández, R., Coll, R. C., Kearney, J., Breit, S. & O'Neill, L. A. J. The intracellular chloride channel proteins CLIC1 and CLIC4 induce IL-1 β transcription and activate the NLRP3 inflammasome. *J. Biol. Chem.* **292**, 12077–12087 (2017).
39. Friard, J. et al. LRRC8/VRAC channels exhibit a noncanonical permeability to glutathione, which modulates epithelial-to-mesenchymal transition (EMT). *Cell Death Dis* **10**, 925 (2019).
40. Zhou, C. et al. Transfer of cGAMP into bystander cells via LRRC8 volume-regulated anion channels augments sting-mediated interferon responses and anti-viral immunity. *Immunity* **52**, 767–781.e6 (2020).
41. Hyzinski-García, M. C., Rudkouskaya, A. & Mongin, A. A. LRRC8A protein is indispensable for swelling-activated and ATP-induced release of excitatory amino acids in rat astrocytes. *J. Physiol.* **592**, 4855–4862 (2014).
42. Gaitán-Peñas, H. et al. Investigation of LRRC8-mediated volume-regulated anion currents in xenopus oocytes. *Biophys. J.* **111**, 1429–1443 (2016).
43. Ferrari, D. et al. Extracellular ATP triggers IL-1 beta release by activating the purinergic P2Z receptor of human macrophages. *J. Immunol.* **159**, 1451–1458 (1997).
44. Di Virgilio, F. Liaisons dangereuses: P2X7 and the inflammasome. *Trends Pharmacol. Sci.* **28**, 465–472 (2007).
45. Baron, L. et al. The NLRP3 inflammasome is activated by nanoparticles through ATP, ADP and adenosine. *Cell Death Dis.* **6**, e1629 (2015).
46. Sil, P. et al. P2Y6 receptor antagonist MRS2578 inhibits neutrophil activation and aggregated neutrophil extracellular trap formation induced by gout-associated monosodium urate crystals. *J. Immunol.* **198**, 428–442 (2017).
47. Uratsuji, H. et al. P2Y6 receptor signaling pathway mediates inflammatory responses induced by monosodium urate crystals. *J. Immunol.* **188**, 436–444 (2012).
48. Lee, G.-S. et al. The calcium-sensing receptor regulates the NLRP3 inflammasome through Ca²⁺ and cAMP. *Nature* **492**, 123–127 (2012).
49. Triantafilou, K., Hughes, T. R., Triantafilou, M. & Morgan, B. P. The complement membrane attack complex triggers intracellular Ca²⁺ fluxes leading to NLRP3 inflammasome activation. *J. Cell Sci.* **126**, 2903–2913 (2013).
50. Gong, T., Yang, Y., Jin, T., Jiang, W. & Zhou, R. Orchestration of NLRP3 inflammasome activation by ion fluxes. *Trends Immunol.* **39**, 393–406 (2018).
51. Yaron, J. R. et al. K⁺ regulates Ca²⁺ to drive inflammasome signaling: dynamic visualization of ion flux in live cells. *Cell Death Dis.* **6**, e1954–e1954 (2015).
52. Camello-Almaraz, C., Gomez-Pinilla, P. J., Pozo, M. J. & Camello, P. J. Mitochondrial reactive oxygen species and Ca²⁺ signaling. *Am. J. Physiol.-Cell Physiol.* **291**, C1082–C1088 (2006).
53. Duranton, C., Huber, S. M. & Lang, F. Oxidation induces a Cl(-)-dependent cation conductance in human red blood cells. *J. Physiol.* **539**, 847–855 (2002).
54. Capó-Aponte, J. E., Iserovich, P. & Reinach, P. S. Characterization of regulatory volume behavior by fluorescence quenching in human corneal epithelial cells. *J. Membr. Biol.* **207**, 11–22 (2005).
55. Untergasser, A. et al. Primer3—new capabilities and interfaces. *Nucleic Acids Res.* **40**, e115 (2012).

Acknowledgements

We thank Pr. T.J. Jentsch (Leibniz-Forschungsinstitut für Molekulare Pharmakologie and Max-Delbrück-Centrum für Molekulare Medizin, Berlin, Germany) for providing the Cx3cr1CreERT2 and Cx3cr1CreERT2/Lrrc8A^{fllox/fllox} mice^{22,23} and his constructive comments during the writing

of the manuscript. We thank Pr. P. Bobé (Université Paris-Saclay, Paris, France) for providing P2X7^{-/-} BMDM. This work was supported by the Laboratory of Excellence: Ion Channel Science and Therapeutics (LabEx ICST, FR), and by grants from the French society of rheumatology (*Société française de rhumatologie*), from Novartis (DREAMER), and from the French National Research Agency (ANR) #ANR-22-CE14-0020 (CRISTAL-in). Figure 7 panel g and Fig. 8 were created with BioRender.com, released under a Creative Commons Attribution-NonCommercial-NoDerivs 4.0 International license <https://creativecommons.org/licenses/by-nc-nd/4.0/deed.en>.

Author contributions

Collection of the human samples (H.K.E., F.L., P.R.); crystal synthesis and characterization (C.C.); measurement of human synovial fluid parameters (T.W.C., M.K., C.C., C.D.); in vivo mouse experiments (T.W.C., C.N.P., H.K.E.); histology studies (T.W.C., C.N.P., M. Z., H.K.E.); generation of THP-1 cell line (V.C., N.L., M.O.); patch-clamp whole cell experiments (M.K., J.F., C.D.); measurement of ATP and IL-1 β by enzymatic method (I.R., M.K., J.F., C.D.); measurement of IL-1 β concentration (M.K., C.N.P., T.W.C., V.C.); western blot analysis, qPCR experiments, generation of cellular clone (LRRC8AKD) and analysis (H.H., N.L., V.C., M.O.); measurement of ATP release using ATP biosensor and time lapse imaging (M.O., F.R., V.C.); data analysis and interpretation (F.R., H.K.E., V.C., C.D.); drafting manuscript (F.R., H.K.E., V.C., C.D.); editing manuscript (F.R., H.K.E., V.C., C.D.).

Competing interests

The authors declare no competing interests.

Additional information

Supplementary information The online version contains supplementary material available at <https://doi.org/10.1038/s41467-024-52543-8>.

Correspondence and requests for materials should be addressed to Vincent Compan, Christophe Duranton or Hang Korng Ea.

Peer review information *Nature Communications* thanks Junya Masumoto and the other, anonymous, reviewer(s) for their contribution to the peer review of this work. A peer review file is available.

Reprints and permissions information is available at <http://www.nature.com/reprints>

Publisher's note Springer Nature remains neutral with regard to jurisdictional claims in published maps and institutional affiliations.

Open Access This article is licensed under a Creative Commons Attribution-NonCommercial-NoDerivatives 4.0 International License, which permits any non-commercial use, sharing, distribution and reproduction in any medium or format, as long as you give appropriate credit to the original author(s) and the source, provide a link to the Creative Commons licence, and indicate if you modified the licensed material. You do not have permission under this licence to share adapted material derived from this article or parts of it. The images or other third party material in this article are included in the article's Creative Commons licence, unless indicated otherwise in a credit line to the material. If material is not included in the article's Creative Commons licence and your intended use is not permitted by statutory regulation or exceeds the permitted use, you will need to obtain permission directly from the copyright holder. To view a copy of this licence, visit <http://creativecommons.org/licenses/by-nc-nd/4.0/>.

© The Author(s) 2024